

# Kaluza-Klein Towers in the Early Universe: Phase Transitions, Relic Abundances, and Applications to Axion Cosmology

Keith R. Dienes,<sup>1,2,\*</sup> Jeff Kost,<sup>1,†</sup> and Brooks Thomas<sup>3,‡</sup>

<sup>1</sup>*Department of Physics, University of Arizona, Tucson, AZ 85721 USA*

<sup>2</sup>*Department of Physics, University of Maryland, College Park, MD 20742 USA*

<sup>3</sup>*Department of Physics, Lafayette College, Easton, PA 18042 USA*

We study the early-universe cosmology of a Kaluza-Klein (KK) tower of scalar fields in the presence of a mass-generating phase transition, focusing on the time-development of the total tower energy density (or relic abundance) as well as its distribution across the different KK modes. We find that both of these features are extremely sensitive to the details of the phase transition and can behave in a variety of ways significant for late-time cosmology. In particular, we find that the interplay between the temporal properties of the phase transition and the mixing it generates are responsible for both enhancements and suppressions in the late-time abundances, sometimes by many orders of magnitude. We map out the complete model parameter space and determine where traditional analytical approximations are valid and where they fail. In the latter cases we also provide new analytical approximations which successfully model our results. Finally, we apply this machinery to the example of an axion-like field in the bulk, mapping these phenomena over an enlarged axion parameter space that extends beyond that accessible to standard treatments. An important by-product of our analysis is the development of an alternate “UV-based” effective truncation of KK theories which has a number of interesting theoretical properties that distinguish it from the more traditional “IR-based” truncation typically used in the extra-dimension literature.

## I. INTRODUCTION

The presence of additional light scalar degrees of freedom is a common feature of many extensions of the Standard Model (SM). Examples include the QCD axion [1–4], a more general set of axions and axion-like particles [5], majorons [6, 7], familons [8], chameleons [9–12], branons [13], dilatons, and a variety of other string and geometric moduli [14–16]. Scalars of this sort are typically light due to symmetries of the high-scale theory which prevent them from acquiring masses. As a result, masses for these particles must be generated by dynamical processes at lower scales which break these symmetries — often in conjunction with a cosmological phase transition. This dynamics also generically leads to a non-trivial time-dependence for the masses of these fields, the details of which can have a significant impact on their late-time energy densities. Understanding these effects is crucial, since such particles can potentially have a variety of phenomenological and cosmological consequences, both helpful and harmful. Indeed, scalars of this sort can contribute to the total abundances of dark matter or dark energy; induce additional, late periods of reheating after cosmic inflation, potentially resulting in substantially modified cosmologies [17]; prematurely induce matter-domination and/or overclose the universe; and disrupt the formation of light elements through late decays.

While the detailed dynamics of mass generation can have important consequences even in scenarios involv-

ing only a single light scalar, the situation becomes far richer in scenarios involving multiple such fields. Indeed, in cases in which these scalars have the same quantum numbers, the dynamics of mass generation can lead them to experience time-dependent mixing. This mixing in turn leads to a continual redistribution of energy density among the scalars during the mass-generation epoch. Such a redistribution can also have profound effects on the late-time energy densities of these fields, several of which were pointed out in Ref. [18]. Specifically, even in a theory involving only two scalars, such a redistribution can lead their late time abundances to experience either an enhancement or a suppression, depending on the choice of model parameters. Moreover, in certain regimes, the system may experience a parametric resonance which can have further dramatic effects on these abundances. Finally, the system may also experience a “re-overdamping” phenomenon in which its energy density reverts to behaving like vacuum energy at a time after its initial transition from the overdamped to underdamped regime.

A variety of scenarios for new physics predict large numbers of scalar fields with similar quantum numbers. Indeed, such collections of fields emerge naturally from a variety of string constructions [19, 20], from axiverse considerations [21], and more generally from theories with extra dimensions. Of course, many features of such theories are highly model-dependent, including the number of fields present, the form of the mass-squared matrix for these fields (both at very early and at very late times), and the time or temperature scales associated with the dynamical mechanisms for mass generation. However, a given specific new-physics context is likely to lead to certain theoretical structures in which some of these features become fixed. For example, theories in which a

\* [dienes@email.arizona.edu](mailto:dienes@email.arizona.edu)

† [jkost@email.arizona.edu](mailto:jkost@email.arizona.edu)

‡ [thomasbd@lafayette.edu](mailto:thomasbd@lafayette.edu)

scalar propagates in extra spacetime dimensions give rise to infinite numbers of scalar fields which are organized into Kaluza-Klein (KK) towers in which the form of the mass matrix at early times — even prior to the onset of any mass-generating phase transition — is dictated by the geometry of the compactification manifold. Because such KK towers arise generically in scenarios involving compact extra dimensions (such as string theories, supergravity theories, and many other high-scale unification models), the features associated with the cosmological evolution of such KK towers — including the dynamical flow of energy amongst the different KK modes prior to, during, and after cosmological phase transitions — are likely to play an important role in early-universe cosmology.

In this paper we tackle this important question. In particular, we study the early-universe cosmology of a KK tower of scalar fields in the presence of a mass-generating phase transition, focusing on the time-development of the total tower energy density (which determines the relic abundance) as well as its distribution across the different KK modes. On the one hand, this study is critical for understanding the cosmological issues associated with extra spacetime dimensions *per se*. On the other hand, this study also represents an extension of the analysis presented in Ref. [18]. In that analysis, only two scalar fields were considered, but these fields were permitted to experience the most general possible mixings between them. In this analysis, by contrast, the number of scalar fields is infinite but the structure of the KK tower and the interplay between brane and bulk physics imposes a strict mixing structure. A goal of this paper is therefore to understand the consequences of this simultaneous extension in the number of fields and narrowing of the allowed mixing structure.

As we shall see, studying the dynamics of a complete KK tower can be a significant undertaking due to its infinite number of fields — especially in the presence of a non-trivial, time-dependent, mass-generating and mixing-inducing phase transition. Therefore, in this paper, we shall work towards this goal in distinct stages by starting with only one KK mode and then introducing more and more KK excitations into the system. Ultimately, we shall build towards the full, infinite KK tower. In each case, our goal is to trace the flow of energy through the system and to examine the behavior of such quantities as the total late-time energy density as well as its distribution across the available KK modes. Moreover, our goal is to retain as much generality as possible. We shall therefore refrain from specifying the exact nature of our KK tower other than to specify that its constituents are scalars. Our results will therefore be broadly applicable to any of the particular scalar fields listed above.

This paper is organized as follows. In Sect. II, we begin by establishing the context in which we shall be working and review the general properties of our setup. Then, in Sect. III, we begin our study by considering the case of

only a single scalar field undergoing a mass-generating phase transition. In particular, our analysis will extend beyond the usual “adiabatic” and “abrupt” regimes commonly discussed in the literature. In Sect. IV, we then broaden our perspective by considering the case of only the  $N$  lowest-lying KK excitations, where  $N$  is arbitrary but finite. As we shall see, situations with finite  $N$  have a number of properties which render their cosmological evolution somewhat distinct. In Sect. V, we then examine how our system behaves as a function of  $N$  for  $N \gg 1$ , and in Sect. VI we present our results for the full, infinite KK tower. In order to distinguish this case from the large- $N$  case in Sect. V, we shall refer to the KK tower as representing the case with  $N = \infty$ . Until this point, our analysis is completely general and applicable to any scalar field. However, in Sect. VII, we then apply our machinery to the case in which our scalar is an axion or axion-like particle. This allows us to interpret our results within a particular phenomenologically relevant context, and illustrate the significant phenomenological implications that our results can have. Finally, in Sect. VIII, we summarize our main conclusions and discuss further potential consequences of our results.

As evident from this outline, our method for studying the properties of a full KK theory involves truncating the KK tower to its  $N$  lowest-lying modes and then considering the  $N \rightarrow \infty$  limit. Indeed, this is a valid, standard approach. However, as a by-product of our analysis, we shall discover that such a truncation is not unique. Specifically, we shall develop an alternate, “UV-based” effective truncation of KK theories which has a number of interesting theoretical properties that distinguish it from the more traditional “IR-based” truncation typically used in the extra-dimension literature. Both truncations lead to the same physics as  $N \rightarrow \infty$ , but differ significantly for finite  $N$ . This alternate truncation will be discussed in Sect. VB.

## II. THE FRAMEWORK

In this section, we establish the framework in which our analysis will take place. This framework is similar to that considered in Refs. [22–25], and is essentially a KK-oriented extension of the framework considered in Ref. [18]. Specifically, we consider a flat, five-dimensional spacetime geometry of the form  $\mathcal{M} \times S^1/\mathbb{Z}_2$ , where  $\mathcal{M}$  denotes our usual four-dimensional Minkowski spacetime and where  $S^1/\mathbb{Z}_2$  denotes an orbifolded circle (*i.e.*, a line segment) of length  $2\pi R$ . Our spacetime coordinates shall be denoted  $(x^\mu, x^5)$ ,  $\mu = 0, 1, 2, 3$ , where  $0 \leq x^5 \leq 2\pi R$  and where the orbifold action is given by  $x^5 \rightarrow -x^5$ . We shall further imagine that our usual Standard-Model (SM) fields and interactions are confined to a four-dimensional brane localized at the orbifold fixed point at  $x^5 = 0$ .

Within this geometry we consider a five-dimensional scalar field  $\Phi(x^\mu, x^5)$  and a corresponding five-

dimensional action  $\mathcal{S}$  of the form

$$\mathcal{S} = \int d^4x dx^5 [\mathcal{L}_{\text{bulk}}(\Phi) + \delta(x^5)\mathcal{L}_{\text{brane}}(\psi_i, \Phi)] \quad (2.1)$$

where  $\psi_i$  are fields confined to the SM brane. In general, our bulk action will contain generic kinetic and mass terms of the form

$$\mathcal{L}_{\text{bulk}}(\Phi) = \frac{1}{2}\partial_M\Phi^*\partial^M\Phi - \frac{1}{2}M^2|\Phi|^2. \quad (2.2)$$

However, many well-motivated scalars such as moduli and axions have a primordial shift symmetry under which  $\Phi \rightarrow \Phi + c$  for arbitrary constants  $c$ . With this motivation in mind, we shall henceforth assume that  $M = 0$ .

The brane Lagrangian  $\mathcal{L}_{\text{brane}}$ , on the other hand, includes the SM Lagrangian in addition to interactions between  $\Phi$  and the SM fields. In general, these interactions can open up decay channels from  $\Phi$  to SM states. However, such interactions can also lead an *effective* four-dimensional mass for  $\Phi$  on the brane. Such masses are typically generated as the result of some brane-localized dynamics (such as a brane-localized phase transition) which occurs at some time during the cosmological evolution on the brane and which explicitly breaks the shift symmetry. For this reason, we shall allow our brane Lagrangian to include a time-dependent effective brane-mass term of the form

$$\frac{1}{\mathcal{V}}\mathcal{L}_{\text{brane}}(\Phi) = -\frac{1}{2}m^2(t)|\Phi|^2 + \dots \quad (2.3)$$

where  $\mathcal{V} \equiv 2\pi R$  is the compactification volume. The behavior of  $m(t)$  is ultimately determined by the details of the non-perturbative dynamics on the brane and thus highly model-dependent.

This information alone is sufficient to allow us to determine the effective four-dimensional theory that emerges upon compactification. Assuming that  $\Phi$  has even parity under the orbifold action  $x^5 \rightarrow -x^5$ , we may perform a Kaluza-Klein expansion of the form

$$\Phi(x^\mu, x^5) = \frac{1}{\sqrt{\mathcal{V}}}\sum_{k=0}^{\infty} r_k \phi_k(x^\mu) \cos\left(\frac{kx^5}{R}\right) \quad (2.4)$$

with normalization constants  $r_0 = 1$  and  $r_k = \sqrt{2}$  for all  $k > 0$ , as appropriate for a  $S^1/\mathbb{Z}_2$  compactification. Inserting this into our action and integrating over  $x^5$  we obtain an effective four-dimensional action of the form

$$\mathcal{L}_{\text{eff}} = \sum_{k=0}^{\infty} \left[ \frac{1}{2}(\partial_\mu\phi_k)^2 - \frac{1}{2}\sum_{\ell=0}^{\infty} \phi_k \mathcal{M}_{k\ell}^2(t)\phi_\ell \right] + \dots \quad (2.5)$$

where our time-dependent mass matrix  $\mathcal{M}_{k\ell}^2$  is given by

$$\begin{aligned} \mathcal{M}_{k\ell}^2 &= k\ell\delta_{k\ell}M_c^2 + r_k r_\ell m^2(t) \\ &= m^2(t) \begin{bmatrix} 1 & \sqrt{2} & \sqrt{2} & \cdots \\ \sqrt{2} & 2 + \frac{M_c^2}{m^2(t)} & 2 & \cdots \\ \sqrt{2} & 2 & 2 + \frac{4M_c^2}{m^2(t)} & \cdots \\ \vdots & \vdots & \vdots & \ddots \end{bmatrix} \end{aligned} \quad (2.6)$$

with  $M_c \equiv 1/R$ . The first term in the top line of Eq. (2.6) represents the expected KK contribution from the physics in the bulk, while the second term reflects the contribution from physics on the brane which breaks the translational symmetry in the  $x^5$ -direction and thereby introduces a mixing between the different KK modes.

Given the Lagrangian in Eq. (2.5), it follows that in a flat Friedman-Robertson-Walker (FRW) spacetime the zero-momentum modes of the KK scalars  $\phi_k$  obey the coupled equations of motion

$$\ddot{\phi}_k + 3H(t)\dot{\phi}_k + \sum_{\ell=0}^{\infty} \mathcal{M}_{k\ell}^2(t)\phi_\ell = 0 \quad (2.7)$$

where  $H(t) \equiv \kappa/(3t)$  is the Hubble parameter. Note that  $\kappa = 2$  and  $\kappa = 3/2$  for matter- and radiation-dominated epochs, respectively. If  $\mathcal{M}_{k\ell}^2$  were constant as a function of time, it would be possible to pass to a mass-eigenstate basis  $\{\phi_\lambda\}$  in which the different differential equations in Eq. (2.7) would decouple. Unfortunately, the time-dependence of  $m(t)$  leads to a time-dependence for  $\mathcal{M}_{k\ell}^2$ . This time-dependence induces an unavoidable mixing between the different modes, since even the mass-eigenstate basis is continually changing. It is this feature which underpins the non-trivial dynamics we shall be studying in this paper. Likewise, at any moment in time, the total energy density associated with our system of KK modes is given by

$$\rho = \frac{1}{2}\sum_k \dot{\phi}_k^2 + \frac{1}{2}\sum_{k,\ell} \phi_k \mathcal{M}_{k\ell}^2 \phi_\ell. \quad (2.8)$$

If the mass matrix  $\mathcal{M}_{k\ell}^2$  were time-independent, it would be possible to rewrite this energy density in the mass-eigenstate basis as the sum of individual contributions:

$$\rho = \sum_\lambda \rho_\lambda \quad (2.9)$$

where

$$\rho_\lambda = \frac{1}{2}\left(\dot{\phi}_\lambda^2 + \lambda^2\phi_\lambda^2\right). \quad (2.10)$$

Unfortunately, once again, the time-dependence of the mass matrix renders such a decomposition impossible. Thus, we may consider the total energy density in Eq. (2.8) as receiving contributions from individual mass eigenstates as in Eq. (2.9) only during those periods of cosmological evolution for which the mass matrix might not be changing with time.

In general, we shall assume that the mass  $m(t)$  is generated through some sort of phase transition on the brane whose occurrence is centered at some time  $t_G$  in cosmological history and which requires a duration  $\Delta_G$  over which to unfold. We shall therefore assume that  $m(t) = 0$  long before the phase transition (*i.e.*, for  $t \ll t_G$ ), while we shall assume that  $m(t)$  is given by some fixed mass  $\bar{m}$  long after the phase transition (*i.e.*, for  $t \gg t_G$ ). The

precise details of how  $m(t)$  evolves from 0 to  $\bar{m}$  clearly depend on the particular structure of the phase transition in question, but we shall find that the most important feature of this function will be its “width”  $\Delta_G$ . For concreteness, we shall therefore adopt the function [18]

$$m(t) = \frac{1}{2} \bar{m} \left\{ 1 + \operatorname{erf} \left[ \frac{1}{\sqrt{2}\delta_G} \log \left( \frac{t}{t_G} \right) \right] \right\}, \quad (2.11)$$

where  $\bar{m}$  is the mass at asymptotically late times, where  $t_G$  is the central time defined by  $m(t_G) = \bar{m}/2$ , and where ‘erf’ denotes the so-called “error” function. In Eq. (2.11), the quantity  $\delta_G \in [0, 1]$  is a dimensionless parameter describing the “width” of the phase transition, with  $\delta_G = 0$  corresponding to an essentially instantaneous phase transition and  $\delta_G = 1$  describing a phase transition which proceeds as slowly as possible. Given the dimensionless parameter  $\delta_G$ , the physical timescale  $\Delta_G$  over which the phase transition occurs is then given by [18]

$$\Delta_G \equiv \sqrt{2\pi}\delta_G t_G. \quad (2.12)$$

Indeed, given Eq. (2.11), we may view the transition from  $m = 0$  to  $m = \bar{m}$  as occurring over a “width”  $\Delta_G$  logarithmically centered at  $t_G$ .

This choice of function is discussed more fully in Ref. [18]. Indeed, it is shown in Ref. [18] that this function models the time-dependence of a variety of phase transitions extremely well in the neighborhood of  $t_G$ , where the mass function is changing most rapidly. This includes the instanton-induced phase transition that gives mass to the QCD axion. Of course, as discussed in Refs. [26–29], the actual QCD phase transition leads to a mass function  $m(t)$  which exhibits a power-law dependence on  $t$  at early times  $t \ll t_G$ , and which is then often taken to be followed by one or more slope discontinuities near  $t \sim t_G$  before becoming a constant for  $t \gg t_G$ . By contrast, our functional form for  $m(t)$  is designed to interpolate smoothly between fixed early- and late-time values in such a way that there is an adjustable and easily identifiable “width”  $\Delta_G$ . Despite these differences, however, it is shown in Ref. [18] that our functional form models the QCD functional form extremely well near  $t \sim t_G$ .

Of course, many other choices are possible for the particular functional form of  $m(t)$ , with different choices being more or less suitable in different contexts. However, none of the qualitative results of this paper will ultimately depend on these specific details.

In general, we may choose to consider phase transitions with any  $\delta_G \leq 1$ . Indeed, as discussed in Ref. [18], situations with  $\delta_G > 1$  suffer from an unphysical boundary artifact near  $t \approx 0$ , namely the emergence of a “fake” mass-generating phase transition whose width tends to decrease as  $\delta_G$  increases beyond  $\delta_G = 1$ . However, when  $\bar{m}/M_c \gg 1$ , it turns out that an additional boundary effect emerges which restricts  $\delta_G$  even more strongly, ultimately imposing an upper limit on  $\delta_G$  which is less than 1 and which depends on  $\bar{m}/M_c$ . (Specifically, as  $\delta_G$  increases for  $\bar{m}/M_c \gg 1$ , the effective “mixing angle”

$\theta$  between our ground state and the first excited state starts changing, evolving from  $\theta = 0$  to  $\theta = \bar{\theta}$  more and more rapidly and at earlier and earlier times. Ultimately we reach a new critical value of  $\delta_G$  beyond which the  $\theta$ -width  $\Delta_\theta$  in Eq. (4.3) of Ref. [18] actually starts to *decrease* when  $\delta_G$  is increased, giving the appearance of a new “fake” phase transition at early times near  $t \approx 0$ .) Avoiding this unphysical behavior then imposes an additional upper bound on  $\delta_G$  which we can evaluate numerically as a function of  $\bar{m}/M_c$  and  $N$ . In this paper we shall therefore restrict our attention to situations with  $\delta_G \leq 1$  but also impose this additional constraint as appropriate for large  $\bar{m}/M_c$ .

In this context, we note that theories with extra spacetime dimensions must generally obey additional “normalcy-temperature” constraints [30, 31] which are more easily satisfied within cosmological low-temperature reheating (LTR) scenarios in which inflation occurs late and reheating occurs at temperatures as low as  $T_{\text{RH}} \sim \mathcal{O}(\text{MeV})$  [32]. If we assume the dynamics that generate  $m(t)$  are at higher scales than  $T_{\text{RH}}$ , then our mass-generating phase transition can be assumed to occur during an inflaton-dominated — *i.e.*, a matter-dominated — epoch. However this assumption will not play a significant role in our analysis, and the primary results of this paper will hold regardless of the specific cosmological timeline assumed.

Given the differential equations of motion in Eq. (2.7), the only ingredients of our model remaining to be specified are the initial conditions on each field mode  $\phi_k$ . While in principle many possibilities exist, the existence of the shift symmetry  $\Phi \rightarrow \Phi + c$  prior to mass generation on the brane suggests that  $\Phi$  might have an arbitrary fixed displacement at early times  $t_i \ll t_G$ , with a fixed non-zero vacuum expectation value (VEV)  $\langle \Phi \rangle \neq 0$ . Upon KK reduction, this corresponds to initial conditions given by

$$\begin{aligned} \phi_k(t_i) &= \langle \phi_0 \rangle \delta_{0k} \\ \dot{\phi}_k(t_i) &= 0, \end{aligned} \quad (2.13)$$

where  $\langle \phi_0 \rangle \equiv \sqrt{2\pi R} \langle \Phi \rangle$ . We shall therefore take these to be the initial conditions for our differential equations (2.7) in what follows. It is important to note that these initial conditions have several additional advantages beyond their natural origins outlined above. First, as long as the initial time  $t_i$  is sufficiently prior to  $t_G$ , our ensemble of KK modes will have zero energy. Thus, as we shall see, *all energy accrued by our KK system is solely the result of the phase transition on the brane*. Moreover, these initial conditions, being essentially static, free our system and its subsequent dynamics from all details concerning the generation of the initial VEV  $\langle \Phi \rangle$ . As a result, the time at which the initial VEV  $\langle \Phi \rangle$  is generated is arbitrary and we need not concern ourselves with its origins. Indeed, as we shall see, the precise value of  $t_i$  will not affect our analysis, or any of our conclusions. Finally, we remark that while  $\langle \phi_0 \rangle$  sets an overall energy scale, this



scale will be irrelevant for our purposes since the equations of motion are linear and our main interest will be on relative *comparisons* between energy scales rather than their absolute magnitudes.

Finally, let us discuss the masses of the individual KK modes in this model. Even though our overall brane mass  $m(t)$  is continually changing in time, diagonalizing the matrix in Eq. (2.6) at any moment in time leads directly to the corresponding instantaneous (mass)<sup>2</sup> eigenvalues  $\lambda_k^2$ . While no closed-form analytical expressions for these eigenvalues exist, they may be readily approximated in the  $m/M_c \ll 1$  and  $m/M_c \gg 1$  limits. In the  $m/M_c \ll 1$  limit, we find

$$\lambda_k \approx \begin{cases} m & k = 0 \\ kM_c & k > 0. \end{cases} \quad (2.14)$$

There are two ways to interpret this result. If we imagine holding  $M_c$  fixed, this limit corresponds to taking  $m$  extremely small. This renders the brane irrelevant in the KK mass decomposition, and indeed the results in Eq. (2.14) are then the eigenvalues expected from a straightforward compactification on a circle. Alternatively, if we imagine holding  $m$  fixed, we see that this limit corresponds to taking  $M_c$  extremely large. We then have only a single light mode with mass  $\lambda_0 \approx m$ , which is nothing but the four-dimensional limit. By contrast, for  $m/M_c \gg 1$ , the mixing between the modes is maximized and our corresponding eigenvalues are given by [22, 23]

$$\lambda_k \approx (k + 1/2) M_c. \quad (2.15)$$

It is remarkable that the effect of the brane mass in this limit is entirely  $m$ -independent, and merely amounts to shifting our eigenvalues by  $M_c/2$ . Indeed, these shifted eigenvalues are those that would have emerged from an *anti*-periodic compactification on a circle. Finally, for intermediate values of  $m/M_c$ , we find that our eigenvalues  $\lambda_k$  tend to follow Eq. (2.15) for  $k \ll \pi m^2/M_c^2$  and Eq. (2.14) for  $k \gg \pi m^2/M_c^2$ , with  $\lambda_k$  taking values that smoothly evolve between these two extremes for other values of  $k$ .

It is important to stress that this behavior for the eigenvalues emerges only in the limit in which we consider the full KK tower with its infinite complement of KK modes,  $k = 0, 1, \dots, \infty$ . By contrast, if we truncate the mass matrix in Eq. (2.6) to its first  $N$  rows and columns so that  $0 \leq \{k, \ell\} \leq N - 1$ , our general expectations described above continue to apply only for the eigenvalues  $\lambda_0, \dots, \lambda_{N-2}$ . However, for the highest eigenvalue  $\lambda_{N-1}$ , we find that the above expectations continue to apply only for  $m^2/M_c^2 \lesssim \mathcal{O}(\sqrt{N})$ . By contrast, for  $N \gg 1$  and for  $m^2/M_c^2 \gtrsim \mathcal{O}(\sqrt{N})$ , we instead find that

$$\lambda_{N-1} \approx \sqrt{2N} m. \quad (2.16)$$

The normalized eigenvalue  $\lambda_{N-1}/M_c$  thus diverges as  $m/M_c \rightarrow \infty$ .

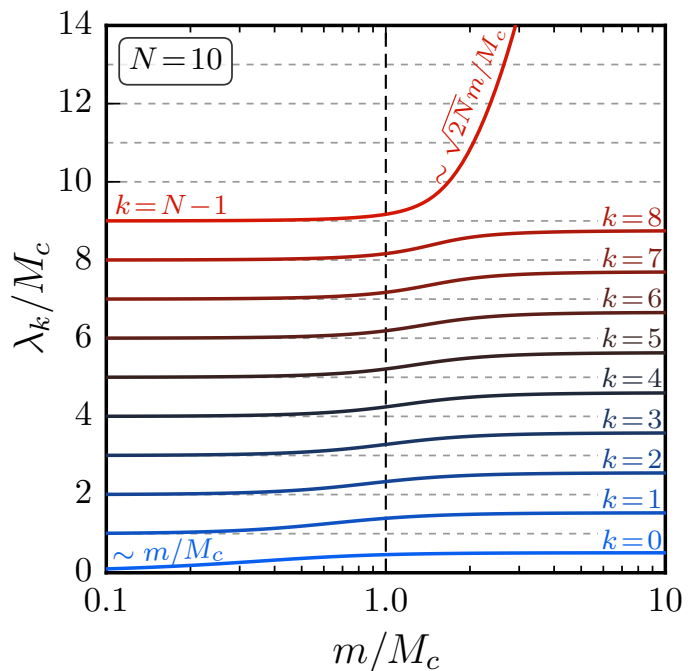


FIG. 1. The mass spectrum  $\lambda_k$  for  $N = 10$ , plotted as a function of  $m/M_c$ . When  $\bar{m} \ll M_c$ , our mass eigenvalues follow the simple form given in Eq. (2.14). By contrast, when  $\bar{m} \gg M_c$ , all but the highest mass eigenvalue shift upwards by  $M_c/2$ , while the highest mass eigenvalue diverges according to Eq. (2.16) for  $m^2/M_c^2 \gtrsim \mathcal{O}(\sqrt{N})$ . As discussed in the text, this anomalous behavior of the highest mass eigenvalue is an artifact of having truncated our KK tower to only a finite number of states, and disappears as  $N \rightarrow \infty$ .

The behavior of the eigenvalues  $\lambda_k$  is illustrated in Fig. 1, where we have plotted the values of  $\lambda_{k=0,\dots,9}$  as functions of  $m/M_c$  for  $N = 10$ . As is clear from Fig. 1, the somewhat anomalous behavior of  $\lambda_{N-1}$  is ultimately an artifact of truncating our KK tower to its first  $N$  values. However, as  $N$  increases, this anomalous behavior of  $\lambda_{N-1}$  sets in only at increasingly large values of  $m/M_c$ . Thus, in the  $N \rightarrow \infty$  limit, this anomalous behavior disappears altogether, as expected.

In our model the quantity  $m$  is generally time-dependent, rising from zero to some final, fixed late-time value  $\bar{m}$  as the result of our mass-generating phase transition on the brane. The corresponding eigenvalues  $\lambda_k^2$  are thus set by Eq. (2.14) with  $m = 0$  at early times, but subsequently evolve towards late-time results which are governed by the magnitude of the late-time ratio  $\bar{m}/M_c$ . Meanwhile, each of the corresponding KK fields  $\phi_k$  is evolving according to Eq. (2.7), with the non-diagonal mass matrix  $\mathcal{M}_{k\ell}^2$  inducing a time-dependent mixing between the KK modes and even between their instantaneous mass eigenstates. This, coupled with the continuously decreasing Hubble friction term  $H(t)$  in Eq. (2.7), leads to a highly non-trivial dynamical system, with energy slowly being introduced into the system as the result of the mass-generating phase transition while it is simul-

taneously and continually redistributed across the different modes and dissipated from each mode. Understanding this energy flow is critical if we are to properly understand the cosmological implications of such KK scalar towers in the presence of mass-generating phase transitions in the early universe. This is therefore the main task to which we now turn.

### III. $N = 1$ : MAPPING OUT THE 4D LIMIT

We begin our analysis by focusing on the simplest case: that of only one scalar field, *i.e.*, the case with  $N = 1$ . This case lacks any dependence on  $M_c$ , and therefore can be considered equivalent to a four-dimensional limit in which  $M_c \gg m(t)$  at all times (so that all KK modes with  $k \geq 1$  effectively decouple from the problem). This case of a single scalar field  $\phi(t)$  undergoing a mass-generating phase transition has been studied extensively in the literature (see, *e.g.*, Refs. [33, 34]), but only in certain “adiabatic” or “abrupt” limits. In this section, by contrast, we shall provide a complete mapping of the entire relevant parameter space.

In general, given the equation of motion in Eq. (2.7), we see that the field  $\phi(t)$  simply follows the trajectory of a damped harmonic oscillator with time-dependent critical damping coefficient  $\zeta \equiv 3H/2m$ . Such an oscillator is overdamped if  $\zeta > 1$  and only experiences oscillations in the underdamped regime with  $\zeta < 1$ . Since  $H(t) \sim \kappa/(3t)$  is monotonically decreasing while  $m(t)$  is monotonically increasing, we see that  $\zeta$  is constantly decreasing. As a result, the field  $\phi(t)$  is necessarily overdamped at times  $t \ll t_G$  and does not begin to undergo coherent oscillations until  $\zeta = 1$ . We shall let  $t_\zeta$  denote this time at which such coherent oscillations begin. In general, we know that  $t_\zeta$  cannot come too much earlier than  $t_G$  (*i.e.*, we cannot have  $t_G - t_\zeta \gg \Delta_G$ ) since our field  $\phi$  is presumed massless prior to the onset of the phase transition. Likewise, if  $t_\zeta$  occurs long after the phase transition has already occurred (*i.e.*, if  $t_\zeta - t_G \gg \Delta_G$ ), the specific details of the phase transition such as its shape or width will have a negligible effect on the resulting dynamics and on the corresponding energy density  $\rho$ . However, if  $|t_\zeta - t_G| \lesssim \Delta_G$ , the specific properties of the phase transition can be significant.

Two approximations are typically used in the literature in order to estimate the effects of the phase transition within this third regime. Both rest upon considering extreme limits of the phase-transition width  $\Delta_G$ . If the width is large enough so that  $\dot{m}/m \ll m$  at all times during the field oscillations (*i.e.*, at all times after  $t_\zeta$ ), then the field undergoes many oscillations during the phase transition. This is the so-called *adiabatic approximation*: the fields remain virialized during the phase transition and we can approximate the energy density by

$$\rho_{4D}(t) \approx \frac{1}{2} \langle \phi_0 \rangle^2 m(t_\zeta) m(t) \left[ \frac{a(t_\zeta)}{a(t)} \right]^3 \quad (3.1)$$

where  $a(t) \sim t^{\kappa/3}$  is the cosmological scale factor. By contrast, if the phase transition width  $\Delta_G$  is extremely small, we are in the so-called *abrupt approximation*: our assumption that  $|t_\zeta - t_G| \lesssim \Delta_G$  forces  $t_\zeta$  and  $t_G$  to coincide, and the phase transition happens so rapidly that the field  $\phi(t)$  retains its initial value  $\langle \phi_0 \rangle$  until  $t_G$  (or equivalently  $t_\zeta$ ), at which point it immediately begins oscillating coherently. The evolution of the energy density is then easily obtained by solving Eq. (2.7) with  $N = 1$  analytically. This yields the exact solution

$$\rho_{4D}(t) = \frac{\pi^2}{8} \langle \phi_0 \rangle^2 \bar{m}^4 \frac{t_G^{\kappa+1}}{t^{\kappa-1}} [B_1^2(t) + B_2^2(t)] \quad , \quad (3.2)$$

where

$$\begin{aligned} B_1(t) &\equiv J_{\kappa_+}(\bar{m}t_G)Y_{\kappa_-}(\bar{m}t) - J_{\kappa_-}(\bar{m}t)Y_{\kappa_+}(\bar{m}t_G) \\ B_2(t) &\equiv J_{\kappa_+}(\bar{m}t)Y_{\kappa_+}(\bar{m}t_G) - J_{\kappa_+}(\bar{m}t_G)Y_{\kappa_+}(\bar{m}t) \end{aligned} \quad (3.3)$$

and where we have defined  $\kappa_\pm \equiv (\kappa \pm 1)/2$ . Note that in both Eq. (3.1) and Eq. (3.2), the quantity  $t$  is measured against the same cosmological clock that measures  $t_G$ .

While the approximations above are applicable in two limits of parameter space, it is important to understand the behavior of the late-time energy density over the entire parameter space. In particular, although the mass-generating phase transition generally pumps energy into the system, and although this energy density is ultimately dissipated by the Hubble friction that slowly damps the resulting field oscillations, it turns out that there can be an additional source of dissipation and therefore an additional source of suppression of the late-time energy density  $\bar{\rho}_{4D}$  compared to our usual expectations based on the abrupt approximation. This arises if the corresponding field is undergoing oscillations *during* the phase transition, while the mass of the field is changing appreciably.

It is easy to identify those regions of parameter space for which this will be the case. In general, there are two criteria that must be satisfied if the scalar field is to undergo at least one oscillation while the mass of the field is changing appreciably. First, the scalar field must indeed be undergoing oscillations at some point during the phase transition — *i.e.*, our system must be in the underdamped regime before the mass of our field reaches  $\bar{m}$ . We thus must have  $3H \lesssim 2\bar{m}$ , or equivalently  $\bar{m}t_G \gtrsim \kappa/2$ , where we have taken  $t_G$  as a rough benchmark time for the phase transition. Second, in order to ensure that at least one or more field oscillations occur during the interval over which the mass is changing, we require that the timescale associated with the field oscillations be shorter than the phase-transition timescale associated with the changing mass. The former timescale is generally given by  $2\pi/m$  and thus decreases throughout the phase transition, ultimately reaching a minimum value  $2\pi/\bar{m}$ , while the latter timescale is nothing but  $\Delta_G$ . As a rough benchmark, our phase transition will therefore include at least one oscillation so long as  $\Delta_G \gtrsim 2\pi/\bar{m}$ , or equivalently

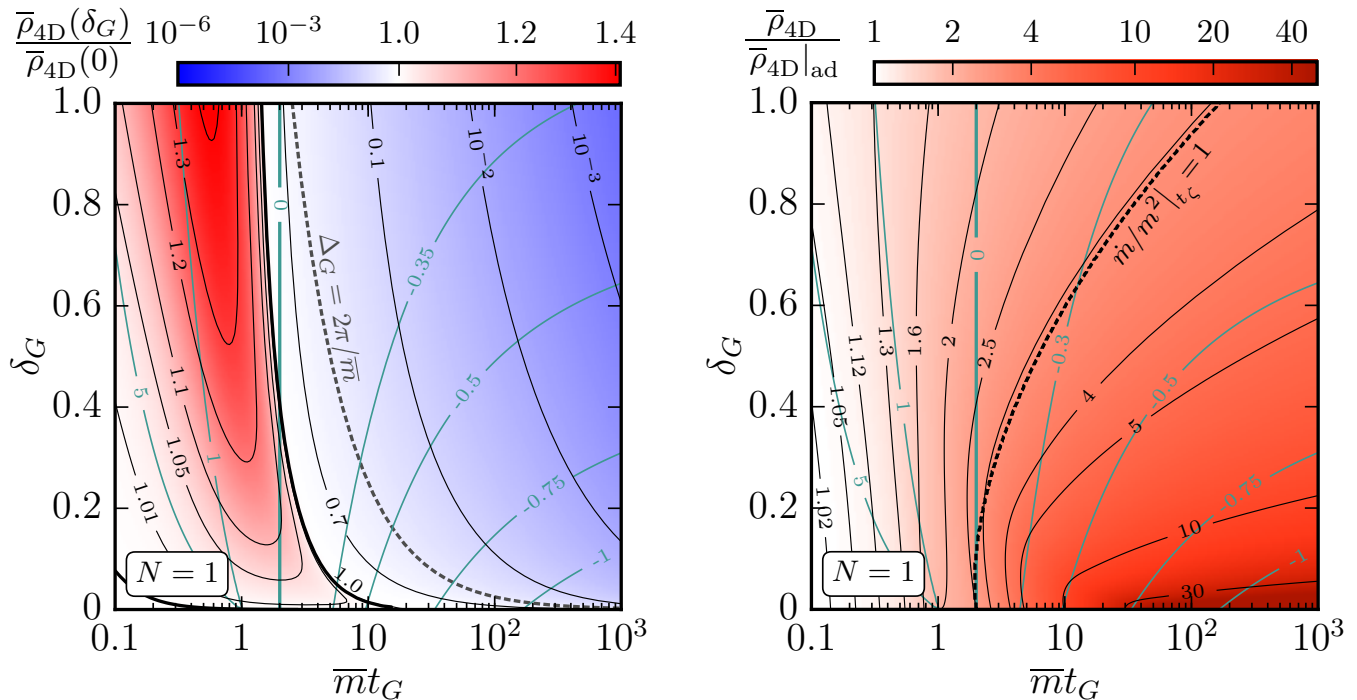


FIG. 2. The late-time energy density  $\bar{\rho}_{4D}$ , plotted within the  $(\bar{m}t_G, \delta_G)$  plane and normalized to the value it would have had in the abrupt approximation (left panel) or adiabatic approximation (right panel). In each case the colors and black lines indicate the contours of the normalized  $\bar{\rho}_{4D}$  (*i.e.*, the degrees to which the true late-time energy density is enhanced or suppressed relative to its approximated value), while the blue lines indicate the corresponding contours of  $(t_\zeta - t_G)/\Delta_G$ . As additional relevant guidelines, the dashed line in the left panel indicates the contour along which  $\Delta_G = 2\pi/\bar{m}$ , while in the right panel it indicates the contour along which  $\dot{m}(t_\zeta) = m^2(t_\zeta)$ . In general, the energy densities in regions above or to the left of these guidelines in the left (right) panel tend to obey the abrupt (adiabatic) approximation more strongly than those below or to the right. We also find that neither approximation holds across the majority of the parameter space shown, with the true values of the late-time energy density  $\bar{\rho}_{4D}$  often experiencing significant suppressions (blue regions) or enhancements (red regions) as compared with the approximated expectations.

$\bar{m}t_G \gtrsim \sqrt{2\pi}/\delta_G$ . Combining our two conditions, we thus find that an additional suppression of the late-time energy density compared with what we might expect based on the abrupt approximation will occur as long as our system satisfies the rough benchmark criterion

$$\bar{m}t_G \gtrsim \max \left\{ \frac{\sqrt{2\pi}}{\delta_G}, \frac{\kappa}{2} \right\}. \quad (3.4)$$

Note that for a matter- or radiation-dominated background cosmology, the underdamped condition will automatically be satisfied whenever the oscillation condition is satisfied.

In the left panel of Fig. 2, we plot the exact numerical value of the late-time energy-density ratio  $\bar{\rho}_{4D}(\delta_G)/\bar{\rho}_{4D}(0)$  within the  $(\bar{m}t_G, \delta_G)$  plane. For reference, the benchmark contour with  $\Delta_G = 2\pi/\bar{m}$  is also plotted. In general, the regions above and to the right of this contour (*i.e.*, regions with  $\bar{m}t_G \gg 1$ ) indeed experience suppressions which grow increasingly severe compared with what we might expect from the abrupt approximation. As indicated in Fig. 2, these are regions with  $t_\zeta > t_G$ . Surprisingly, however, we note that there

is also a region in which the late-time energy density is *enhanced* compared with its abrupt expectation. This region arises only for  $\bar{m}t_G \sim \mathcal{O}(1)$ , and typically has  $t_\zeta - t_G \lesssim \Delta_G$ . Like the corresponding suppression, this too is a feature of considering a non-zero timescale for the phase transition, occurring only when  $\delta_G > 0$ . Finally, for  $\bar{m}t_G \ll 1$  or for  $\delta_G \ll 1$ , we see that our late-time energy density is neither enhanced nor suppressed. Indeed, these are the regions in which the abrupt approximation applies.

In the right panel of Fig. 2, we plot the same late-time energy density  $\bar{\rho}_{4D}(\delta_G)$ , only now normalized to what we might expect from the *adiabatic* approximation. In this case, the contour with  $\dot{m}/m^2 = 1$  at  $t = t_\zeta$  is shown as a relevant guideline. Unlike the comparison to the abrupt approximation, in this case we see that the late-time energy density  $\bar{\rho}_{4D}(\delta_G)$  is *enhanced* throughout the entire region with  $\delta_G > 0$ . As expected, this enhancement is relatively mild in regions to the left of the  $\dot{m}/m^2 = 1$  contour but grows increasingly severe below and to the right. Once again, it is only for  $\bar{m}t_G \ll 1$  that the adiabatic approximation appears to hold.

We see, then, that our usual expectations based on

the abrupt or adiabatic approximations apply only in relatively small regions of the full  $(\overline{m}t_G, \delta_G)$  parameter space, the former consisting of the regions with  $\overline{m}t_G \ll 1$  or  $\delta_G \ll 1$  and the latter consisting of the region with  $\overline{m}t_G \ll 1$ . Interestingly, we see that *either* approximation yields the same (reliable) result for  $\overline{m}t_G \ll 1$ , regardless of the value of  $\delta_G$ . In all other regions, however, we see that these standard approximations break down — often significantly — with the adiabatic approximation tending to underestimate the true value and the abrupt approximation either under- or over-estimating the true value, depending on the particular values of  $\overline{m}t_G$  and  $\delta_G$ .

One of the advantages of the abrupt and/or adiabatic approximations is that they provide relatively simple, *analytical* expressions for the late-time energy density  $\overline{\rho}_{4D}(\delta_G)$ . Unfortunately, as we have seen, these expressions are accurate only within relatively narrow slices of the full parameter space. Given this deficiency, we now offer two approximate analytical expressions for  $\overline{\rho}_{4D}(\delta_G)/\overline{\rho}_{4D}(0)$  which together describe its numerical values fairly accurately across the entire parameter space shown in Fig. 2. Subsequent use of the analytical expression in Eq. (3.1) then allows us to isolate  $\overline{\rho}_{4D}(\delta_G)$ .

We begin by noting that within the suppressed region in the left panel of Fig. 2, the contours of  $\overline{\rho}_{4D}(\delta_G)/\overline{\rho}_{4D}(0)$  roughly follow the same slope as the contour with  $\Delta_G = 2\pi/\overline{m}$ . Indeed, for  $\delta_G \lesssim 0.3$ , one finds the approximate power-law scaling behavior

$$\frac{\overline{\rho}_{4D}(\delta_G)}{\overline{\rho}_{4D}(0)} \sim \frac{1}{\overline{m}t_G\delta_G}. \quad (3.5)$$

Of course, as we move closer to the  $\delta_G = 1$  boundary, the contours deviate from this scaling behavior and the suppression grows increasingly severe. Nevertheless, we find an approximate expression

$$\frac{\overline{\rho}_{4D}(\delta_G)}{\overline{\rho}_{4D}(0)} \approx \frac{(\overline{m}t_G\delta_G)^{-0.92}}{1 + [(\overline{m}t_G)^{1/4} - 3/2] \delta_G^2} \quad (3.6)$$

which holds to within  $\pm 20\%$  across the entire suppressed region and which approximately reduces to the power-law result in Eq. (3.5) for very small  $\delta_G$ .

By contrast, turning to the enhanced region near  $\overline{m} \sim 1/t_G$ , we see the maximum of this enhancement always occurs at  $\delta_G = 1$ . Indeed, we find that we can approximate this enhancement analytically in the Gaussian form

$$\frac{\overline{\rho}_{4D}(\delta_G)}{\overline{\rho}_{4D}(0)} \approx 1 + 0.42 \exp \left[ -\mathbf{v}^T \begin{pmatrix} 1.64 & 0.68 \\ 0.68 & 0.67 \end{pmatrix} \mathbf{v} \right], \quad (3.7)$$

where  $\mathbf{v} \equiv [\log(\overline{m}t_G/0.54), \log(\delta_G)]^T$ . In this case, the error associated with this approximation is bounded to lie between  $-10\%$  and  $5\%$  throughout the non-suppressed portion of the parameter space shown. Thus, with the analytical expressions in Eq. (3.6) and Eq. (3.7), we now cover the entire single-scalar parameter space. We shall nevertheless continue to use our exact results throughout the rest of this paper.

In Fig. 2 we have presented our results for the late-time energy density  $\overline{\rho}_{4D}$  as fractions of the values this quantity would have had in either the abrupt or adiabatic approximations. These results therefore enabled us to understand the effects that can accrue beyond the regions in which these approximations are valid. However, it is also important to consider the *absolute* magnitudes of  $\overline{\rho}_{4D}$  that are generated throughout our  $(\overline{m}t_G, \delta_G)$  parameter space. These can be trivially obtained at each point in parameter space by multiplying the results in the left panel of Fig. 2 by the corresponding values in Eq. (3.2) [or equivalently the results in the right panel of Fig. 2 by the corresponding values in Eq. (3.1)].

The results are shown in Fig. 3, where we plot the absolute magnitude of  $\overline{\rho}_{4D}$  in units of  $\frac{1}{2}\langle\phi\rangle^2 t^{-2}$ . Once again,  $t$  refers to universal time, measured against the same cosmological clock as  $t_G$ . Thus, for example, if our late-time mass is chosen to be  $\overline{m}t_G = 10$  and our mass-generating phase transition width is chosen to be  $\delta_G = 0.4$ , we find from Fig. 3 that our resulting late-time energy density  $\overline{\rho}_{4D}$  is given approximately as

$$\overline{\rho}_{4D}(t) \approx 50 \langle\phi\rangle^2 t^{-2}. \quad (3.8)$$

In general, we see from Fig. 3 that our late-time energy density  $\overline{\rho}_{4D}$  is independent of  $\delta_G$  for

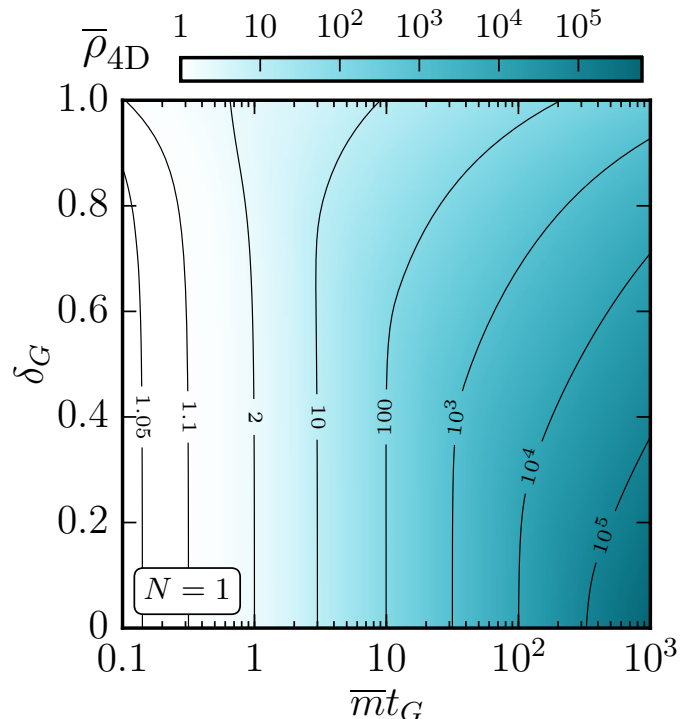


FIG. 3. The *absolute* late-time energy density  $\overline{\rho}_{4D}$ , plotted in units of  $\frac{1}{2}\langle\phi\rangle^2 t^{-2}$  within the  $(\overline{m}t_G, \delta_G)$  plane. Note that our late-time energy density  $\overline{\rho}_{4D}$  is generally independent of  $\delta_G$  for  $\{\overline{m}t_G \lesssim 10^3, \delta_G \lesssim 0.5\}$  and scales roughly as  $(\overline{m}t_G)^2$  within this region.



$\{\overline{m}t_G \lesssim 10^3, \delta_G \lesssim 0.5\}$  and moreover scales roughly as

$$\overline{\rho} \sim (\overline{m}t_G)^2 \quad (3.9)$$

for  $\overline{m}t_G \gtrsim 1$ . Of course, this scaling behavior extends to larger and larger values of  $\overline{m}t_G$  as  $\delta_G \rightarrow 0$ , as we expect from the abrupt approximation.

#### IV. $N > 1$ : A GENERAL STUDY WITH MULTIPLE FIELDS

We now consider how these results evolve as we move away from the  $N = 1$  limit and consider larger, arbitrary values of  $N$ . Note that although we will eventually be considering the  $N \rightarrow \infty$  limit, the theories we analyze here with finite  $N > 1$  are interesting in their own right, as will be discussed further in the Conclusions. As discussed in Sect. II, taking  $N > 1$  introduces not only additional  $\phi$  fields (each potentially with its own critical oscillation time  $t_c$ ) but also the non-trivial *mixing* between these fields that is a consequence of the mass-generating phase transition on the brane (resulting in a non-diagonal squared-mass matrix  $\mathcal{M}_{k\ell}^2$ ). Systems with  $N > 1$  can therefore be expected to be considerably more complex than their simpler  $N = 1$  cousins.

Towards this end, we shall concentrate not only on the behavior of the *total* late-time energy density  $\overline{\rho}$  but also on its *distribution* across the different  $\phi$  fields. As discussed in Sect. II, one cannot resolve the individual contributions to the total energy density  $\rho$  during times when the mass matrix is appreciably changing, since the non-vanishing time-derivatives of  $\mathcal{M}_{k\ell}^2$  introduce new terms into  $\rho$  which prevent its simple decomposition into the form in Eq. (2.9). However, at late times  $t$  for which  $(t - t_G)/\Delta_G \gg 1$  — *i.e.*, at times when the phase transition is largely completed — the corresponding mass matrix  $\mathcal{M}_{k\ell}^2$  becomes essentially time-independent. The mass-eigenstate fields  $\phi_\lambda$  then decouple from each other and virialize. At such late times, a decomposition such as that in Eq. (2.9) becomes possible, with each such late-time energy density contribution  $\rho_\lambda$  given in Eq. (2.10). Thus, in order to characterize the late-time energy configuration of the system with  $N$  fields, we can calculate not only  $\overline{\rho}$  but also the individual contributions  $\overline{\rho}_\lambda$  corresponding to the  $N$  individual mass eigenstates  $\phi_\lambda$ .

Finally, following Ref. [23], another useful quantity we may define is the so-called *tower fraction*  $\eta$ . This quantity measures the fraction of the total energy density which is carried by all but the most abundant mode in the tower:

$$\overline{\eta} \equiv 1 - \max_\lambda \left\{ \frac{\overline{\rho}_\lambda}{\overline{\rho}} \right\}. \quad (4.1)$$

For large but finite  $N$ , the tower fraction  $\eta$  takes values within  $0 \leq \eta < 1$  and can be viewed as quantifying the extent to which our system really has multiple components, with each carrying some relevant portion of the total energy density. If  $\eta$  is extremely close to zero, then

almost all of the total energy density is captured within a single field, rendering the other fields largely irrelevant from a phenomenological point of view. For this reason we shall be most interested in systems with larger values of  $\eta$ .

Given this, we shall analyze the general- $N$  system by tracing its energy flow, moment by moment through the mass-generating phase transition, ultimately evaluating the total late-time energy density  $\overline{\rho}$ , its distribution across the individual contributions  $\overline{\rho}_\lambda$ , and the corresponding late-time value of  $\overline{\eta}$  — all as functions of  $m$ ,  $M_c$ ,  $t_G$ , and  $\delta_G$ .

##### A. Instantaneous phase transition

It turns out that we can actually perform this calculation analytically in the special abrupt-transition limit  $\delta_G \rightarrow 0$ . Indeed, in this limit our mass matrix  $\mathcal{M}_{k\ell}^2$  is time-independent both before and after  $t_G$ , and all that we need calculate is the sudden change of basis from the KK-eigenstate basis  $\phi_k$  which is appropriate before  $t_G$  to the mass-eigenstate basis  $\phi_\lambda$  which is appropriate after. Prior to  $t_G$ , only  $\phi_{k=0}$  has an initial displacement  $\langle \phi_0 \rangle$ : this field is massless prior to  $t_G$ , and thus the system has no energy and none of the fields oscillate. However, for times after  $t_G$ , our mass eigenstates  $\phi_\lambda$  become

$$\phi_\lambda = \sum_{k=0}^{N-1} U_{\lambda k} \phi_k \quad (4.2)$$

where  $U_{\lambda k}$  is the time-independent but  $N$ -dependent unitary basis-change matrix that diagonalizes  $\mathcal{M}_{k\ell}^2$ . The initial conditions in Eq. (2.13) then become

$$\begin{aligned} \phi_\lambda(t_G) &= U_{\lambda 0} \langle \phi_0 \rangle \\ \dot{\phi}_\lambda(t_G) &= 0, \end{aligned} \quad (4.3)$$

whereupon our total energy density at  $t = t_G$  is given by

$$\begin{aligned} \rho(t_G) &= \sum_\lambda \rho_\lambda(t_G) = \frac{1}{2} \sum_\lambda \lambda^2 \phi_\lambda^2 \\ &= \frac{1}{2} \sum_\lambda \lambda^2 U_{\lambda 0}^2 \langle \phi_0 \rangle^2. \end{aligned} \quad (4.4)$$

However, for all  $N$ , our basis-change matrix  $U_{\lambda k}$  satisfies the remarkable identity

$$\sum_\lambda \lambda^2 U_{\lambda 0}^2 = m^2 \quad (4.5)$$

which completely eliminates from  $\rho(t_G)$  what has otherwise been a highly non-trivial dependence on  $M_c$  (and  $N$ ). We thus find that our phase transition at  $t = t_G$  injects into our  $N$ -mode system a total energy density

$$\rho(t_G) = \frac{1}{2} m^2 \langle \phi_0 \rangle^2, \quad (4.6)$$

with individual fractional contributions

$$\frac{\rho_\lambda(t_G)}{\rho(t_G)} = \left( \frac{\lambda}{m} \right)^2 U_{\lambda 0}^2. \quad (4.7)$$

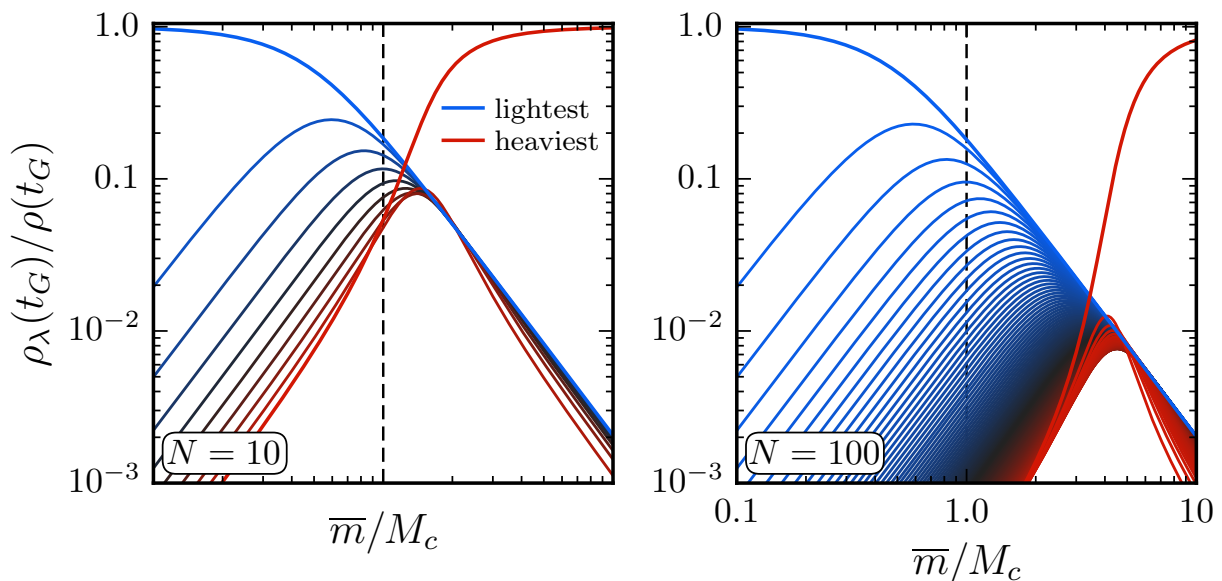


FIG. 4. The abundance fractions  $\rho_\lambda/\rho$  at time  $t = t_G$ , evaluated within the abrupt  $\delta_G \rightarrow 0$  limit and plotted as functions of  $\bar{m}/M_c$  for  $N = 10$  (left panel) and  $N = 100$  (right panel). In both panels we observe that the lightest mode carries the largest fractional abundance for small  $m/M_c$ , but that this abundance is more fully distributed amongst the modes as  $m/M_c$  increases. For finite  $N$ , this abundance then ultimately collects in the *heaviest* mode as  $m/M_c \rightarrow \infty$ . This last feature is ultimately an artifact of the truncation to only finitely many modes, and disappears in the  $N \rightarrow \infty$  limit. In all cases, the sum of the fractional abundances shown is equal to 1 for all  $m/M_c$ .

Note that because we are working in the abrupt  $\delta_G \rightarrow 0$  limit, the mass  $m$ , eigenvalues  $\lambda$ , and basis-change matrix  $U_{\lambda k}$  in Eqs. (4.2) through (4.7) are constant for all times after  $t_G$  and thus equal to their late-time values:  $m = \bar{m}$ ,  $\lambda = \bar{\lambda}$ , and  $U_{\lambda k} = \bar{U}_{\lambda k}$ .

In general, we see from Eq. (4.6) that the total energy density injected into our system grows polynomially with  $m$ . However, the individual contributions to this total energy density vary non-trivially as a function of  $m/M_c$  — even when expressed as a fraction relative to the total. These individual fractional contributions to the total energy density at  $t = t_G$  are plotted as functions of  $m/M_c$  for  $N = 10$  in the left panel of Fig. 4 and for  $N = 100$  in the right panel of Fig. 4. In each case, we see that these energy-density distributions are highly sensitive to  $m/M_c$ , with the majority of the energy density at  $t = t_G$  carried by the lightest mode for small  $m/M_c$  (as consistent with our expectation from the 4D limit). However, as  $m/M_c$  increases, this picture changes, with more and more of the states beginning to carry greater fractions of the total energy density. Note that for all values of  $m/M_c$ , the sum of these fractional energy densities is fixed at 1.

Ultimately, for very large  $m^2/M_c^2 \gtrsim \mathcal{O}(\sqrt{N})$ , the majority of the energy density begins to collect in the *heaviest* mode. However, we have already seen in Sect. II that this is precisely the regime in which the heaviest eigenvalue  $\lambda_{N-1}$  begins to diverge. Indeed, as discussed in Sect. II, this feature is ultimately an artifact of truncating our system to a finite number of modes, with  $N < \infty$ .

A similar situation persists for the corresponding energy densities. Even though the energy density associated with the heaviest mode tends to dominate in the region with  $m^2/M_c^2 \gtrsim \mathcal{O}(\sqrt{N})$ , this region becomes increasingly remote as  $N \rightarrow \infty$  and effectively vanishes. Thus, for  $m/M_c \gg 1$  and  $N \rightarrow \infty$ , all of the modes in our theory tend to share the total energy density essentially equally.

In Fig. 5 we show the corresponding values of the tower fraction  $\eta(t)$  at  $t = t_G$ , plotted as functions of  $m/M_c$ . As we see,  $\eta(t_G)$  is non-monotonic as a function of  $m/M_c$  for all finite values of  $N$ , starting near  $\eta \approx 0$  for small  $m/M_c$  and reaching a maximum at a certain critical  $N$ -dependent value  $(m/M_c)_{\text{peak}}$  before declining back to  $\eta \approx 0$  for large  $m/M_c$ . This non-monotonic behavior for finite  $N$  is ultimately a result of the fact that the identity of the mode carrying the maximum abundance is itself a function of  $m/M_c$ , with the lightest mode carrying the largest abundance for small  $m/M_c$  but the heaviest mode carrying the largest abundance for large  $m/M_c$ . However, as  $N \rightarrow \infty$ , we find that the magnitude of the peak tends towards unity while the position of peak itself shifts towards increasingly large values of  $m/M_c$ . Indeed, with excellent precision, we find that the position of the peak is given by

$$\left(\frac{m}{M_c}\right)_{\text{peak}} \approx \frac{4}{9} N^{4/9}, \quad (4.8)$$

whereupon it follows that  $(m/M_c)_{\text{peak}} \rightarrow \infty$  as  $N \rightarrow \infty$ . We thus find that  $\eta(t_G)$  becomes completely monotonic in the infinite- $N$  limit, transitioning from  $\eta \approx 0$  at small

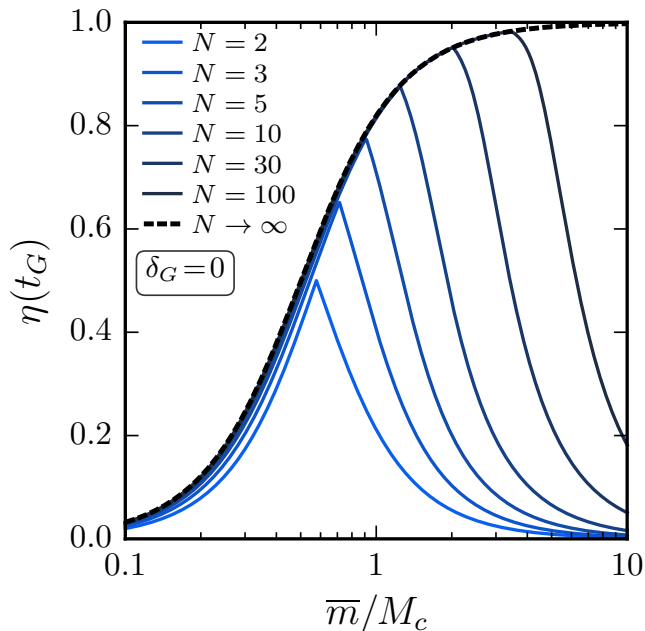


FIG. 5. The tower fractions  $\eta(t_G)$  corresponding to the fractional abundances shown in Fig. 4, plotted as functions of  $m/M_c$  for different values of  $N$ . We see that the tower fraction begins near zero for small  $m/M_c$  but then begins to grow as  $m/M_c$  increases. For finite  $N$ , the tower fraction ultimately hits a peak before returning to zero at large  $m/M_c$ , while in the  $N \rightarrow \infty$  limit the tower fraction continues monotonically to 1.

$m/M_c$  to  $\eta \approx 1$  at large  $m/M_c$ .

The results illustrated in Fig. 4 and 5 apply to the energy configuration of our system at  $t = t_G$ . A natural question, however, concerns the extent to which these results apply for the *late-time* energy-density fractions  $\bar{\rho}_\lambda/\bar{\rho}$  and late-time tower fraction  $\bar{\eta}$ . Even though the mass matrix  $M_{k\ell}^2$  and associated eigenvalues are time-independent for all  $t > t_G$  in the abrupt  $\delta_G \rightarrow 0$  limit, the mass eigenstates  $\phi_\lambda(t)$  and corresponding energy densities  $\rho_\lambda(t)$  nevertheless continue to have a non-trivial time-dependence. In general, a single field  $\phi_\lambda$  with constant mass  $\lambda$  remains essentially fixed for all  $t < t_\zeta^{(\lambda)} \equiv \kappa/(2\lambda)$  and then transitions to damped-oscillatory behavior for  $t > t_\zeta^{(\lambda)}$ . Likewise, the corresponding energy density is essentially fixed for  $t < t_\zeta^{(\lambda)}$  and then decays as  $t^{-\kappa}$  for  $t > t_\zeta^{(\lambda)}$ . (Exact analytical results for the fields and energy densities can be found in Appendix A and Fig. 1 of Ref. [18].) Thus, in our present situation with an abrupt phase transition at  $t = t_G$ , all of our fields will already be underdamped and commence oscillations simultaneously at  $t_G$  as long as  $t_\zeta^{(\lambda)} \leq t_G$  for all  $\lambda$ . In such cases, the ratios  $\rho_\lambda/\rho$  as well as the corresponding tower fraction  $\eta$  will be essentially time-independent, with the same values at late times as they have at  $t_G$ .

## B. Phase transition with arbitrary width $\delta_G$

The results given above apply only in the abrupt  $\delta_G \rightarrow 0$  limit. However, we now wish to explore the full parameter space and calculate our total and fractional late-time energy densities and tower fractions throughout the  $(\bar{m}t_G, \delta_G)$  plane. We already did this for the  $N = 1$  limiting case in Sect. III, where we found that the effects of taking  $\delta_G > 0$  tended to produce either suppressions or enhancements in the resulting late-time energy  $\bar{\rho}_{4D}(\delta_G)$  compared with  $\rho_{4D}(0)$  depending on the precise values of  $\bar{m}t_G$  and  $\delta_G$ . These results were shown in the left panel of Fig. 2. We therefore now seek to know what additional effects beyond those in Fig. 2 emerge from considering arbitrary values of  $N$  rather than merely  $N = 1$ .

Our results are shown in Fig. 6 for  $t_G = 10^2/M_c$ . Remarkably, for that portion of the  $(\bar{m}t_G, \delta_G)$  parameter space with  $\bar{m}t_G \lesssim 10$ , we find that the total late-time energy density  $\bar{\rho}$  is virtually identical to what it would have been for only one mode! Of course, this behavior is consistent with what we already saw for the abrupt  $\delta_G \rightarrow 0$  limit and very small  $m/M_c$ , but what is remarkable is that this behavior extends even for non-zero  $\delta_G$  and larger  $m/M_c$  as well. Moreover, for  $\bar{m}t_G \gtrsim 10$ , we find that our late-time energy density is actually suppressed rather than enhanced relative to our 4D expectations — all this despite the presence of extra modes whose masses are also lifted by (and which therefore also receive an additional energy-density insertion from) the mass-generating phase transition.

These results may be understood as follows. Since we have taken  $t_G = 10^2/M_c$  as a reference value, we see that  $\bar{m}t_G = 10^2 \bar{m}/M_c$ . Thus values  $\bar{m}t_G \lesssim 10^2$  correspond to  $\bar{m}/M_c \lesssim 1$ , and we have already seen that the bulk of the energy density remains concentrated in the lightest mode for such values of  $\bar{m}/M_c$ . As a result, our system is functionally no different than the single-mode 4D system for small values of  $\bar{m}t_G$ . By contrast, as we increase the value of  $\bar{m}t_G$ , the total energy density of our system is more equally distributed across the different modes. The oscillations of the heavier modes then dissipate the energy density more rapidly than the lighter modes during the phase transition, resulting in a more rapid dissipation of the total energy density and thus an overall suppression of the late-time energy density as compared with 4D expectations. It also is important to note that this latter effect requires  $\delta_G > 0$ , even for large  $\bar{m}t_G$ . Indeed, if  $\delta_G = 0$ , our energy density is partitioned across the different modes precisely as described in Sect. IV A, whereupon the unitarity relation in Eq. (4.5) removes all dependence on  $N$  and ensures the same results as we would have had in 4D!

In Fig. 7 we plot the corresponding values of the late-time tower fraction  $\bar{\eta}$ . As evident from this figure, the  $(\bar{m}t_G, \delta_G)$  plane is subdivided into two disjoint  $\bar{\eta} \approx 0$  regions by a fairly narrow “mountain range” along which  $\bar{\eta} > 0$ . As we already determined in Sect. IV A for the  $\delta_G \rightarrow 0$  limit, the region with smaller  $\bar{m}t_G$  (or equiva-

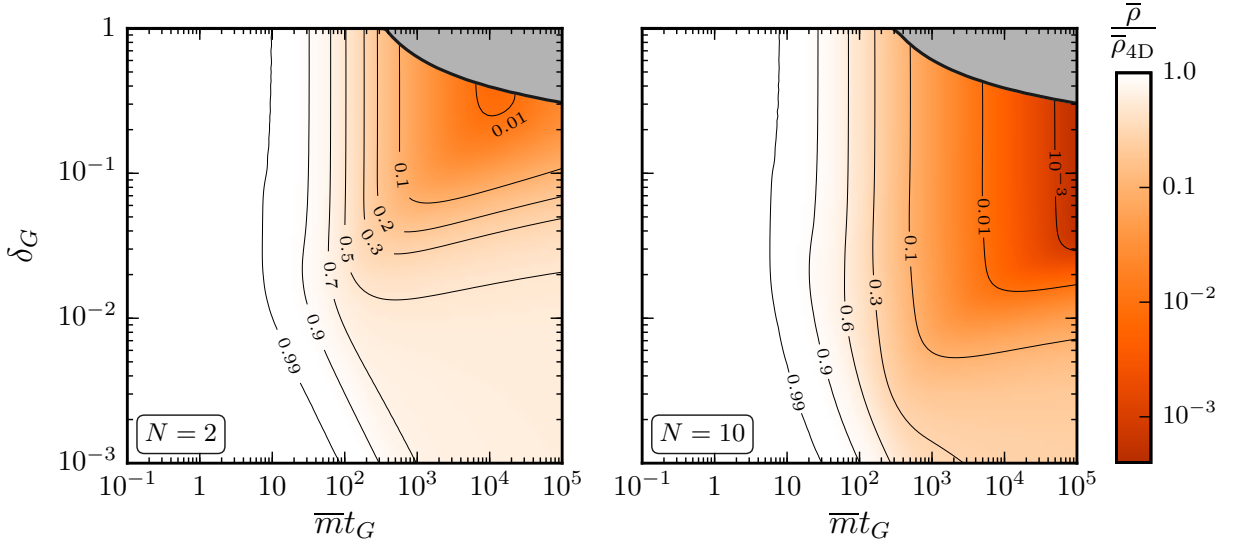


FIG. 6. The total late-time abundance  $\bar{\rho}$  for  $N$  modes, evaluated within the  $(\bar{m}t_G, \delta_G)$  plane for  $N = 2$  (left panel) and  $N = 10$  (right panel) and expressed as a fraction of the corresponding value  $\bar{\rho}_{4D}$  for the 4D  $N = 1$  special case. We have chosen  $t_G = 10^2/M_c$  as a reference value for both plots above. We see that the introduction of additional modes relative to the 4D special case either *preserves* the 4D result nearly exactly for  $\bar{m}t_G \lesssim 10$  or *suppresses* it for  $\bar{m}t_G \gtrsim 10$ , with this suppression becoming increasingly severe for larger  $\bar{m}t_G$  (or equivalently, larger  $\bar{m}/M_c$ ) and  $\delta_G \lesssim 1$ . Note that the gray regions in the upper right corners of these panels (and in similar subsequent figures throughout this paper) are excluded for the reasons discussed in the paragraph below Eq. (2.12).

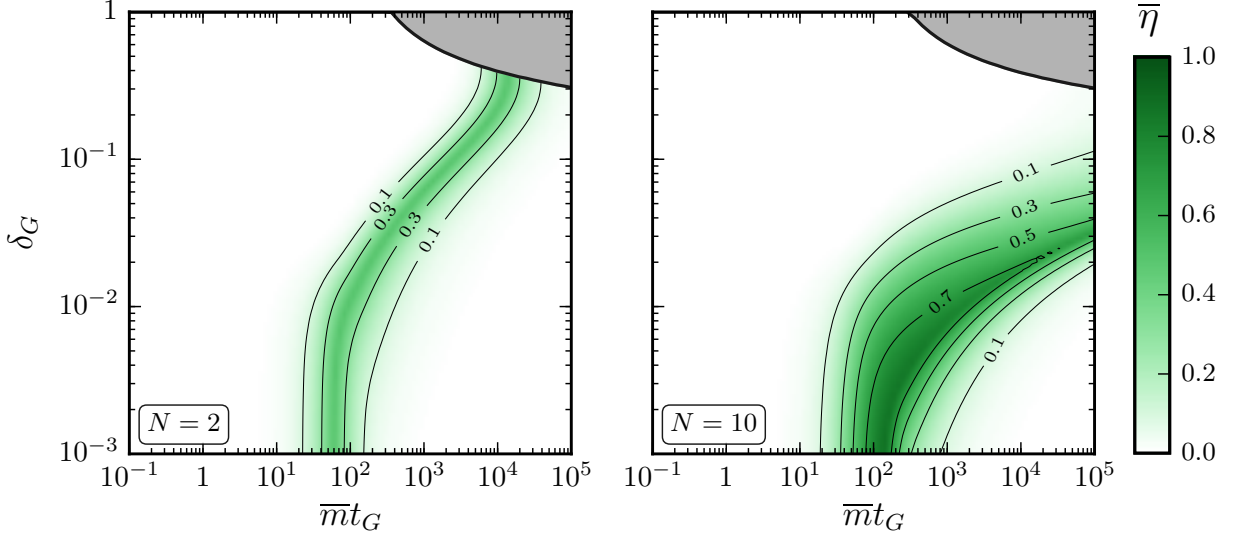


FIG. 7. The total late-time tower fraction  $\bar{\eta}$  corresponding to the panels shown in Fig. 6. In each case we see that the  $(\bar{m}t_G, \delta_G)$  plane is subdivided into two disjoint  $\bar{\eta} \approx 0$  regions (white) by a narrow  $\bar{\eta} > 0$  ribbon (green): the lightest mode carries the bulk of the energy density in the region to the left of the ribbon, while the heaviest mode carries the bulk of the energy density in the region to the right. Interestingly, the division between these two regions is non-monotonic as a function of not only  $\bar{m}t_G$  but also  $\delta_G$ .

lently smaller  $\bar{m}/M_c$ ) corresponds to the region in which the lightest mode carries all of the energy density. By contrast, as we dial  $\bar{m}t_G$  towards greater values, the energy density is increasingly distributed across all the modes, resulting in a greater tower fraction. Ultimately, however, as we dial  $\bar{m}t_G \rightarrow \infty$  in our finite- $N$  system, all

of the energy density finds itself in the heaviest mode, and the tower fraction returns to zero. This behavior is consistent with that shown in Fig. 5 for the  $\delta_G \rightarrow 0$  limit.

This explains the non-monotonicity of the late-time tower fraction  $\bar{\eta}$  as a function of  $\bar{m}t_G$ . However, we additionally learn from Fig. 7 that the late-time tower frac-



tion is also non-monotonic as a function of  $\delta_G$ . This too is relatively straightforward to explain. For  $\bar{m}t_G$  sufficiently large and for small  $\delta_G$ , we have already seen that the bulk of the energy density is carried by the heaviest mode. However, as we increase  $\delta_G$ , we are increasing the timescale associated with our phase transition — *i.e.*, the timescale over which energy is pumped into the system and each mode becomes populated. Eventually this timescale reaches the timescale associated with the oscillations of the heaviest mode. This then suppresses the energy transfer into the (nevertheless dominant) heaviest mode, thereby increasing the tower fraction. Indeed, as we increase  $\delta_G$  still further, we begin to suppress the energy densities of lighter and lighter modes, and this too has the effect of increasing the tower fraction. Eventually, however, as we continue to increase  $\delta_G$ , we reach a point where we have suppressed the majority of the modes and the bulk of the energy density begins collecting in the lightest mode. Subsequent increases in  $\delta_G$  then only reinforce the dominance of the lightest mode, thereby causing the tower fraction to return to zero. Indeed, as shown in Fig. 7, we have crossed the green “mountain range”, leaving us in the region in which the lightest mode carries all of the energy density.

Thus far, our discussion has focused on the regime with  $t_G M_c \gg 1$ . In this regime, all of our excited modes are underdamped and have begun oscillating at very early times prior to the phase transition. This will be true even for the lightest mode if  $\bar{m}t_G$  is chosen sufficiently large. However, if  $t_G M_c \ll 1$  and  $N \gtrsim 1/(t_G M_c)$ , only an upper subset of the modes will have begun oscillating prior to the phase transition — the lightest modes will remain overdamped and fixed. Thus, the introduction of the heavier modes relative to the 4D case has the effect of distributing some of the energy density into heavier modes which begin oscillating earlier than the lightest mode, thereby enhancing the dissipation of the total energy density relative to the 4D case. It is important to stress that this source of suppression is completely distinct from that discussed above, resulting instead from differences in the times at which individual modes begin oscillating. As such, this effect — which was originally discussed in Ref. [22] within the context of the abrupt  $\delta_G \rightarrow 0$  limit — is largely independent of  $\delta_G$ .

## V. APPROACHING ASYMPTOTIA: $N \rightarrow \infty$

We now wish to study how our  $N$ -mode system evolves as a function of  $N$ , with an eye towards understanding the asymptotic behavior of our system for large  $N \gg 1$ . This will ultimately enable us to extract the behavior of the full  $N = \infty$  Kaluza-Klein tower, as we shall do in Sect. VI. This will also enable us to understand the effects that come from truncating the KK system to finite but large  $N$ .

### A. Large- $N$ behavior: The road to asymptotia

In Fig. 8, the blue curves indicate the  $N$ -dependence of our two quantities of interest, namely the late-time energy density  $\bar{\rho}$  of our  $N$ -mode system as well as its corresponding late-time tower fraction  $\bar{\eta}$ . While the latter quantity is shown in the right panel, the former is plotted in the left panel as a fraction of the value it would have in the abrupt  $\delta_G \rightarrow 0$  limit and in the middle panel as a fraction of its corresponding 4D value. For all three panels we have taken  $t_G = 10^2/M_c$  and  $\bar{m} = 10^2 M_c$ , thereby fixing  $\bar{m}t_G = 10^4$  as a benchmark value. We have then plotted the resulting curves (blue) as functions of  $N$  for different values of  $\delta_G$ . (By contrast, the red curves will be discussed in Sect. VB.)

As expected, each of the blue curves shown in Fig. 8 eventually heads towards a finite asymptote as  $N \rightarrow \infty$ . One immediate observation from the left and middle panels of Fig. 8 is that increasing the number of modes in our system generally results in an *increasing suppression* of the total late-time energy density when compared to the values this energy density would have in the abrupt  $\delta_G \rightarrow 0$  or 4D limits. Thus, *the larger the value of  $N$ , the more the abrupt and 4D approximations fail to accurately estimate the late-time energy density*. This is an important result, given that most approaches to calculating the energy densities of such multiple-component systems in the literature assume that the phase transition occurs when the fields are still overdamped. Compared with these static fields, any such phase transition is therefore essentially occurring with an infinitely short timescale  $\delta_G$ , and is thereby functionally equivalent to the abrupt approximation. The results shown in Fig. 8 thus illustrate what happens as one moves away from these assumptions.

In this vein, it is perhaps also worthwhile to consider the adiabatic approximation which is traditionally applied in single-component scalar theories undergoing mass-generating phase transitions. Of course, while an adiabatic approximation can be realized for a single mode, we do not expect such an approximation to be appropriate for a large collection of modes with vastly different masses and non-trivial mixings. Despite this, we can nevertheless imagine limiting cases in which all excited modes above the lightest mode are drained of significant energy density. In such a regime we can then imagine applying the adiabatic approximation to the only surviving mode  $\phi_{\lambda_0}$  in the ensemble, leading to a definition

$$\rho(t)|_{\text{ad}} \equiv \frac{1}{2} \langle \phi_0 \rangle^2 \lambda_0(t_\zeta^{(\lambda_0)}) \lambda_0(t) \left[ \frac{a(t_\zeta^{(\lambda_0)})}{a(t)} \right]^3, \quad (5.1)$$

where  $t_\zeta^{(\lambda)}$  is defined as the time at which  $3H(t) = 2\lambda(t)$  and where we implicitly assume  $\delta_G = 1$  when evaluating  $\lambda(t)$ . We have already seen in the left panel of Fig. 2 that the adiabatic approximation sets a lower bound for the energy density associated with a single mode — indeed,

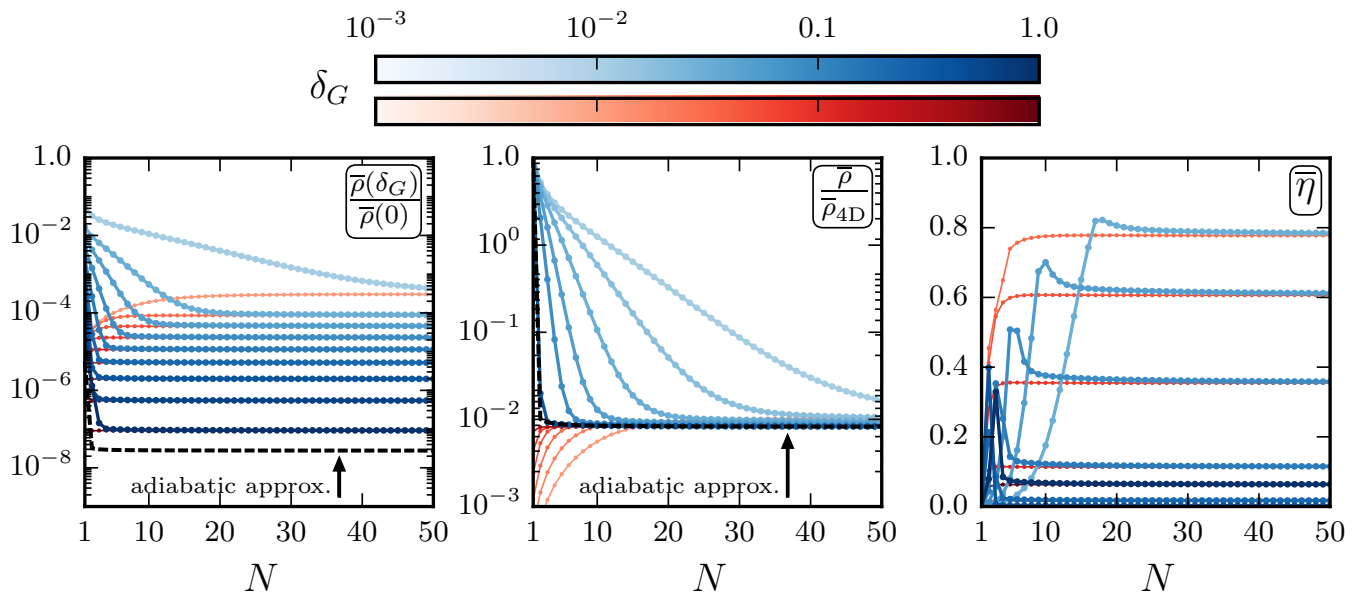


FIG. 8. The total late-time abundance  $\bar{\rho}$  and late-time tower fraction  $\bar{\eta}$  of our  $N$ -mode system, plotted as functions of  $N$  for different values of  $\delta_G$ . The left and center panels show the total late-time abundance expressed as a fraction of the value it would have in the abrupt  $\delta_G \rightarrow 0$  and 4D limits, respectively, while the right panel shows the late-time tower fraction. For all three panels we have taken  $t_G = 10^2/M_c$  and  $\bar{m} = 10^2 M_c$ , thereby fixing  $\bar{m}t_G = 10^4$  as a benchmark value. The blue curves are calculated using the usual “IR-based” truncation which has been employed thus far in Sects. II through IV, while the red curves are calculated using the alternative “UV-based” truncation to be discussed in Sect. VB; both truncations have the same  $N \rightarrow \infty$  asymptotic behavior but the UV-based truncation reaches asymptotia far more rapidly and smoothly. The black-dashed line that occurs in each of the energy-density panels indicates the results of the multi-component adiabatic approximation of Eq. (5.1) which serves as a lower bound for the energy density of the ensemble.

in all other regions of parameter space the energy density is either the same or enhanced. Likewise, the approximation in Eq. (5.1) consists of disregarding whatever energy density might reside in the excited modes. Thus, we expect the adiabatic approximation in Eq. (5.1) to provide us with a lower bound on the total energy density of our  $N$ -mode system throughout all regions of parameter space.

The dashed-black curves in the left and middle panels of Fig. 8 show the behavior of Eq. (5.1) as a function of  $N$ . Indeed, as expected, we see that *the adiabatic approximation serves as a lower bound on the total energy density of the tower*, just as it does in the single-field scenario. Indeed, we see from Fig. 8 that the adiabatic limit seems to be reached most directly for large  $N$  (such as for a full KK tower) and  $\delta_G \rightarrow 1$ . By contrast, the results in other regions of parameter space differ significantly from this limit.

### B. A new truncation of KK theory: An alternate road to asymptotia

Our results in Fig. 8 clearly illustrate a successful road to asymptotia, as each of the blue curves heads towards a finite asymptotic value as  $N \rightarrow \infty$ . This is not a surprise, since we began our analysis by truncating our infinite-

dimensional KK mass matrix  $\mathcal{M}_{k\ell}^2$  in Eq. (2.6) by retaining only its first  $N$  rows and columns. Thus it is natural that taking  $N \rightarrow \infty$  restores the physics of the infinite-matrix limit. Indeed, truncating our mass matrix in Eq. (2.6) to only its first  $N$  rows and columns represents one way of constructing a finite  $N$ -mode theory whose  $N \rightarrow \infty$  limit reproduces the physics of the full KK tower at any moment in time.

However, this is not a unique truncation to a finite  $N$ -mode theory. There is, in fact, an alternative truncation of our full KK theory at any moment in time which also has only  $N$  modes and which also reproduces the physics of the full KK tower as  $N \rightarrow \infty$ , yet yields significantly different physical results for finite  $N$ . Indeed, as we shall see, this alternate truncation exhibits an even more rapid path to asymptotia, yielding what are essentially the full infinite- $N$  values of the late-time energy densities and tower fraction for even smaller values of  $N$  than are required using the standard truncation that we have employed thus far.

Recall that our standard truncation began with the full, infinite-dimensional mass matrix  $\mathcal{M}_{k\ell}^2$  in Eq. (2.6), expressed in the KK basis of the individual KK modes  $\phi_k$ . This matrix was then truncated to its first  $N$  rows and columns. The resulting  $N \times N$  matrix then defined our truncated KK theory, and all subsequent calculations proceeded from this truncated matrix. Specifically, all

calculations were performed directly from the equations of motion (2.7) in the KK basis (which has the advantage of representing a basis choice that does not change with time, even in the presence of the mass-generating phase transition), and the results at late times were converted to the mass-eigenstate basis (such as for quoting late-time quantities such as  $\bar{\rho}_\lambda$  or  $\bar{\eta}$  which pertain to individual mass eigenstates) only at the final step.

However, an alternative approach is *not* to truncate our infinite-dimensional mass matrix in the KK basis  $\phi_k$ , but rather to transform the infinite-dimensional matrix into its mass-eigenstate basis and then truncate the resulting *mass-eigenstate* matrix. In general, this matrix will take the form

$$\mathcal{M}_{\lambda\lambda'}^2 = \begin{pmatrix} \lambda_0^2 & 0 & 0 & \dots \\ 0 & \lambda_1^2 & 0 & \dots \\ 0 & 0 & \lambda_2^2 & \dots \\ \vdots & \vdots & \vdots & \ddots \end{pmatrix}, \quad (5.2)$$

where the  $\lambda_k^2$  are the mass eigenvalues that are calculated in the infinite- $N$  limit at any moment in time. These eigenvalues will be discussed below.

Note that truncating the mass matrix in the mass-eigenstate basis is mathematically different than truncating the mass matrix in the KK-eigenstate basis. Of course, these procedures are in some sense parallel in that they both begin from equivalent infinite-dimensional matrices which describe the same KK system and which are related to each other through a simple, unitary basis change. However, their truncations to  $N \times N$  submatrices are mathematically different, and thus have different physical effects.

Having truncated our mass-eigenstate matrix  $\mathcal{M}_{\lambda\lambda'}^2$  in Eq. (5.2), our final step is to convert the resulting matrix back to the KK basis. In order to do this, we use a similarly truncated version of the exact basis-change matrix  $U_{\lambda k}$  that would have related  $\mathcal{M}_{k\ell}^2$  and  $\mathcal{M}_{\lambda\lambda'}^2$  in the full infinite-dimensional limit. Specifically, we define

$$\widetilde{\mathcal{M}}_{k\ell}^2 \equiv \sum_{\lambda,\lambda'} (\widehat{U}^\dagger)_{k\lambda} \widehat{\mathcal{M}}_{\lambda\lambda'}^2 \widehat{U}_{\lambda'\ell} \quad (5.3)$$

where  $\widehat{\mathcal{M}}_{\lambda\lambda'}^2$  and  $\widehat{U}_{\lambda'\ell}$  here represent the first  $N \times N$  submatrices within the exact infinite- $N$  matrices  $\mathcal{M}_{\lambda\lambda'}^2$  and  $U_{\lambda k}$  respectively. Note that since  $\widehat{U}$  is a truncated version of the unitary infinite- $N$  matrix  $U$ , the truncated matrix  $\widehat{U}$  is not unitary by itself. In particular,  $\widehat{U}$  is *not* the matrix that diagonalizes the new matrix  $\widetilde{\mathcal{M}}_{k\ell}^2$  defined in Eq. (5.3), and thus, strictly speaking, we should not regard  $\widetilde{\mathcal{M}}_{k\ell}^2$  defined in Eq. (5.3) as representing the KK-basis version of  $\widehat{\mathcal{M}}_{\lambda\lambda'}^2$ . We can nevertheless proceed to use  $\widetilde{\mathcal{M}}_{k\ell}^2$  directly in our equations of motion (2.7), treating  $\widetilde{\mathcal{M}}_{k\ell}^2$  as we would any other mass matrix. Converting our final results into statements about individual mass eigenstates at late times is then done in the usual way by diagonalizing  $\widetilde{\mathcal{M}}_{k\ell}^2$  and calculating its mass eigenvalues

and eigenvectors. Note that these eigenvalues will generally differ from the  $\lambda_i$  which appear in the  $\widehat{\mathcal{M}}_{k\ell}^2$  matrix and only approach these  $\lambda_i$  as  $N \rightarrow \infty$ .

Because this alternate truncation of our KK theory utilizes the exact eigenvalues  $\lambda_k$  and exact basis-change matrix elements  $U_{\lambda k}$  corresponding to the full KK theory, it may at first glance seem that this alternate truncation cannot be realized in practice. However, it turns out to be relatively straightforward to solve the eigensystem corresponding to the full infinite-dimensional mass matrix  $\mathcal{M}_{k\ell}^2$  in Eq. (2.6) — not only numerically, but even analytically. One finds [22, 23] that the mass eigenvalues  $\lambda_i$  at any moment in time are the (infinite) set of solutions to the transcendental equation

$$\frac{\pi\lambda}{M_c} \cot\left(\frac{\pi\lambda}{M_c}\right) = \frac{\lambda^2}{m^2}, \quad (5.4)$$

and likewise the corresponding  $U_{\lambda k}$  matrix is given by

$$U_{\lambda k} = \left( \frac{r_k \lambda^2}{\lambda^2 - k^2 M_c^2} \right) A_\lambda \quad (5.5)$$

where the  $r_k$  are defined below Eq. (2.4) and where

$$A_\lambda \equiv \frac{\sqrt{2} m^2}{\lambda \sqrt{\lambda^2 + m^2 + \pi^2 m^4 / M_c^2}}. \quad (5.6)$$

Following the procedure outlined above, we then find that our alternate mass matrix is given by

$$\widetilde{\mathcal{M}}_{k\ell}^2 = \sum_{\lambda=\lambda_0}^{\lambda_{N-1}} \frac{r_k r_\ell A_\lambda^2 \lambda^6}{(\lambda^2 - k^2 M_c^2)(\lambda^2 - \ell^2 M_c^2)}. \quad (5.7)$$

In this connection, we remark that although constructing  $\widetilde{\mathcal{M}}_{k\ell}^2$  requires explicit knowledge of the exact eigenvalues  $\lambda_i$  and matrix elements  $U_{\lambda k}$ , this in no way implies that we have already solved the problems we originally set out to investigate. Indeed, our goals are far deeper than mere KK spectroscopy and instead pertain to understanding the dynamical energy flow within our KK system in the presence of mode-mixing and mass-generating phase transitions.

Although each element of the matrix  $\widetilde{\mathcal{M}}_{k\ell}^2$  in Eq. (5.7) depends on  $N$  explicitly through the upper limit of the  $\lambda$ -summation, this matrix smoothly reproduces our original  $\mathcal{M}_{k\ell}^2$  mass matrix as  $N \rightarrow \infty$ . Indeed, through clever use of the eigenvalue equation (5.4), cotangent summation identities such as

$$\sum_{k=0}^{\infty} \frac{2\lambda^2}{\lambda^2 - k^2 M_c^2} = 1 + \frac{\pi\lambda}{M_c} \cot\left(\frac{\pi\lambda}{M_c}\right), \quad (5.8)$$

and unitarity relations such as that in Eq. (4.5), it is possible to demonstrate explicitly that performing the summation in Eq. (5.7) over the *full* spectrum (*i.e.*, taking  $N \rightarrow \infty$ ) reproduces our original mass matrix in Eq. (2.6), as it must by construction. For example, in

what is perhaps the simplest case, we see from Eq. (5.7) that

$$\widetilde{\mathcal{M}}_{00}^2 = \sum_{\lambda=\lambda_0}^{\lambda_{N-1}} A_\lambda \lambda^2. \quad (5.9)$$

If the summation had proceeded over the entire infinite spectrum, the unitarity relation in Eq. (4.5) would have given us the correct infinite- $N$  result  $\mathcal{M}_{00}^2 = m^2$ . Thus, we see in this case that our UV-based truncation consists of gently draining away the contributions to the unitarity sum that come from the most massive modes, thereby deforming this first matrix element in a gentle,  $N$ -dependent way. Other matrix elements are similar.

The new matrix  $\widetilde{\mathcal{M}}_{k\ell}^2$  in Eq. (5.7) thus defines an alternate truncation of the full KK theory. Indeed, both our original truncated mass matrix  $\mathcal{M}_{k\ell}^2$  in Eq. (2.6) and our new mass matrix  $\widetilde{\mathcal{M}}_{k\ell}^2$  in Eq. (5.7) describe the same KK theory in their  $N \rightarrow \infty$  limits. However, for any finite  $N$  these mass matrices define distinct theories. We shall refer to our traditional truncation as being “IR-based”, since it builds our finite- $N$  theory directly from the ground up, KK mode by KK mode, directly as they were in the full theory without regard for any of the UV physics. By contrast, we shall refer to our alternative truncation as being “UV-based” in the sense that it utilizes the full UV values of the mass eigenvalues and basis-changing matrices prior to truncation, and gently builds these quantities into our recipe for truncation. This is thus more of a “top-down”, UV-sensitive approach. Of course, it is only because of the mixing of KK states induced by the phase transition on the brane that these two truncations are distinct.

What makes this alternate UV-based truncation particularly important for our purposes in this paper is that it provides a much more rapid road to asymptotia than does our usual truncation. In other words, the asymptotic values of late-time quantities such as  $\bar{\rho}_\lambda$  and  $\bar{\eta}$  are approached more rapidly as functions of  $N$  via our UV-based truncation than via the traditional IR-based truncation. We can also see this from Fig. 8. In Fig. 8, the blue curves illustrate the IR-based approach to asymptotia for these quantities. However, in Fig. 8 we have also superimposed the red curves which represent the results of our UV-based approach to asymptotia for these same quantities. In all cases, we see that the UV-based approach to asymptotia tends to differ significantly from the IR-based approach for small  $N$ . Indeed, as  $N$  increases, we see that the finite- $N$  energy densities associated with the IR-based approach tend to approach their asymptotic limits *from above*, while the finite- $N$  energy densities associated with the UV-based approach tend to approach these same asymptotic limits *from below*. Nevertheless, as  $N \rightarrow \infty$ , we see that the UV-based truncation approaches asymptotia more rapidly (for smaller values of  $N$ ) than does the IR-based truncation. We also observe that the approach to asymptotia provided by the UV-based truncation is monotonic, particularly for the

late-time tower fraction  $\bar{\eta}$ , whereas the path provided by the IR-based approach is non-monotonic. However, this too is straightforward to understand. In general, the non-monotonicity of  $\bar{\eta}(N)$  in the IR-based approach is due to the somewhat spurious effects of the highest mass eigenstate in the finite- $N$  system, as discussed in Sect. II and sketched in Figs. 1 and 4. In the UV-based approach, by contrast, the highest mode no longer behaves anomalously for finite  $N$ .

These features are also readily apparent simply by comparing the eigenvalues of the IR-based truncated mass matrix  $\mathcal{M}_{k\ell}^2$  in Eq. (2.6) with those of the UV-based truncated mass matrix  $\widetilde{\mathcal{M}}_{k\ell}^2$  in Eq. (5.7) as functions of  $N$ . Our results are shown in Fig. 9 for  $m/M_c = 2$ . Once again, we see that the asymptotic  $N \rightarrow \infty$  limit is approached more rapidly and more smoothly in the UV-based approach (red curves) than in the IR-based approach (blue curves). Moreover, we see that the anomalous highest eigenvalue which appears in the latter approach no longer exists in the former.

At the end of Sect. V A, we introduced a multi-component adiabatic approximation (5.1) and noted that this quantity provides a lower bound on the total energy

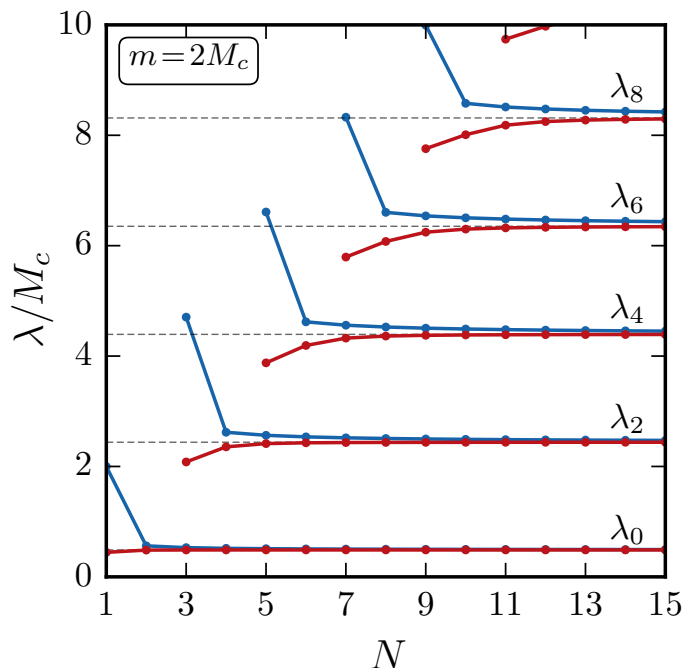


FIG. 9. Eigenvalues of the IR-based and UV-based mass matrices, plotted respectively in blue and red as functions of  $N$  for  $m/M_c = 2$ . For visual clarity, only even eigenvalues are shown. In each case the blue and red curves asymptote to the exact eigenvalues  $\lambda_k$  as  $N \rightarrow \infty$ , but the UV-based red curves generally approach this limit more rapidly and more smoothly than do the IR-based blue curves. Note that each blue curve begins with an anomalously high eigenvalue; this is nothing but the truncation artifact already sketched in Fig. 1 for the highest mode  $\lambda_{N-1}$  in each case. By contrast, such artifacts are entirely eliminated in the UV-based approach.



density of our  $N$ -mode system because it includes only the contributions from the lightest mode. Like other physical finite- $N$  quantities, however, the value of this quantity and its interpretation as a lower limit depend on the specific KK truncation chosen, since the truncation in some sense determines what is meant by the lightest mode and whether its contributions are affected by the removal of the higher modes. This is readily apparent in Fig. 8, where the red “UV-based” values of the total energy density are clearly smaller for certain small values of  $N$  than the “IR-based” values of the adiabatic lower limit. These red “UV-based” total energies nevertheless strictly exceed the values of a corresponding “UV-based” adiabatic lower limit.

We conclude with a final comment. Although we have presented our alternate UV-based truncation of the full KK theory as providing a more rapid road to asymptotia, the existence of such an alternate truncation is interesting in its own right. In any theory involving extra spacetime dimensions, one can never probe all energy scales and thereby detect all KK modes. Instead, we expect the physics of our full KK system to be approximately represented at low energies through some sort of truncation that focuses on the lower modes. *However, if the physics of our extra dimensions results in a mixing of KK modes (as must always arise in any theory which breaks translational invariance in the extra compactified dimension), we now see that there are multiple options for performing such a truncation.* Indeed, one could even argue that our UV-based truncation is more appropriate for certain calculations since it incorporates and thus is more sensitive to the actual masses of the physically propagating mass-eigenstates that we would expect to observe experimentally. This last statement is of course subject to various renormalization-group effects which could potentially deform the observed KK masses and couplings, as discussed in Refs. [35–37], and which exist even for theories such as those considered in Refs. [35–37] in which no KK-mixing is present. These observations nevertheless potentially give our UV-based truncation a theoretical importance in its own right that renders it worthy of further study.

Of course, there does exist a well-defined procedure through which one can unambiguously describe the physics of our full KK theory at low energies: one can use the methods of effective field theory (EFT). Specifically, one carefully integrates out the modes with energies above a particular cutoff scale, thereby obtaining not only a truncated KK tower exhibiting renormalized masses, but also a set of effective operators which reflect the underlying structure of the full theory. In general, the structure of such an EFT can be quite complicated. Thus, it is traditional in the literature to simply adopt the IR-truncated theory as an approximation to this EFT. Our point, then, is that our UV-based truncation might profitably serve as an alternative approximation to the complete EFT — an approximation which, as we have discussed, may have certain advantages. Needless to say, the UV and IR truncations, as

well as the complete EFT, all converge to the full KK theory as  $N \rightarrow \infty$ .

## VI. KK TOWER LIMIT: $N = \infty$

Having studied our system as a function of  $N$  for large  $N \gg 1$ , we are now finally in a position to present our results for the late-time energy density  $\bar{\rho}$  and tower fraction  $\bar{\eta}$  for the full, infinite KK tower. As we shall see, certain features emerge in the full infinite- $N$  limit that were not present for any finite  $N$ . Taken together, these results thus describe the late-time energy configuration across our infinite KK tower when it has been subjected to a mass-generating phase transition of arbitrary width  $\delta_G$  and arbitrary magnitude (set by the late-time brane mass  $\bar{m}$ ) at time  $t_G$  during its cosmological history.

We shall present our results in several different ways. First, in Fig. 10, we plot our results for the total late-time energy density  $\bar{\rho}$  as a fraction of  $\bar{\rho}(\delta_G = 0)$  (left panel) or  $\bar{\rho}_{4D}$  (right panel). Our first observation from the results in Fig. 10 is that while a quantity such as  $\bar{\rho}(\delta_G = 0)$  might indeed be a useful approximation for  $\bar{\rho}$  which is valid in certain regions of parameter space, such an approximation can fail badly in others. For example, we see that the abrupt ( $\delta_G = 0$ ) approximation works well for small  $\bar{m}t_G \lesssim 0.1$  even if  $\delta_G$  is sizable but is otherwise capable of either significantly underestimating or overestimating the true late-time energy density  $\bar{\rho}$ , the latter often by many orders of magnitude.

Another immediate observation is that the contours in Fig. 10 follow a power-law type behavior in those regions of  $(\bar{m}t_G, \delta_G)$  parameter space in which we are eventually going to be the most interested, namely those regions with  $\bar{m}t_G \gtrsim 10$  and  $\delta_G \lesssim 0.3$  in which multiple components contribute non-trivially to the total late-time abundance and  $\bar{\eta} > 0$ . This power-law behavior enables us to extract approximate analytical expressions for  $\bar{\rho}/\bar{\rho}(\delta_G = 0)$  and  $\bar{\rho}/\bar{\rho}_{4D}$  which are valid in these regions. Specifically, given the results in Fig. 10 (as well as analogous results calculated for different values of  $t_G$ ), we find

$$\frac{\bar{\rho}(\delta_G)}{\bar{\rho}(0)} \approx \frac{0.6}{\delta_G} \frac{e^{-\frac{1}{2}M_c/\bar{m}}}{\bar{m}t_G} \left(\frac{M_c}{\bar{m}}\right)^{0.9} \quad (6.1)$$

and

$$\frac{\bar{\rho}}{\bar{\rho}_{4D}} \approx \frac{1}{1 + 2(\bar{m}/M_c)e^{-\frac{1}{2}M_c/\bar{m}}}. \quad (6.2)$$

While the expression in Eq. (6.1) holds to within  $\pm 25\%$  across the relevant  $\bar{\eta} > 0$  region, this result is actually somewhat sensitive to the value of  $t_G$ , with the upper error limit growing smaller with increasing  $t_G$  and bigger with decreasing  $t_G$ . By contrast, the expression in Eq. (6.2) holds to within  $\pm 5\%$  across the relevant region, making it one of the most accurate analytical approximations we have presented in this paper.

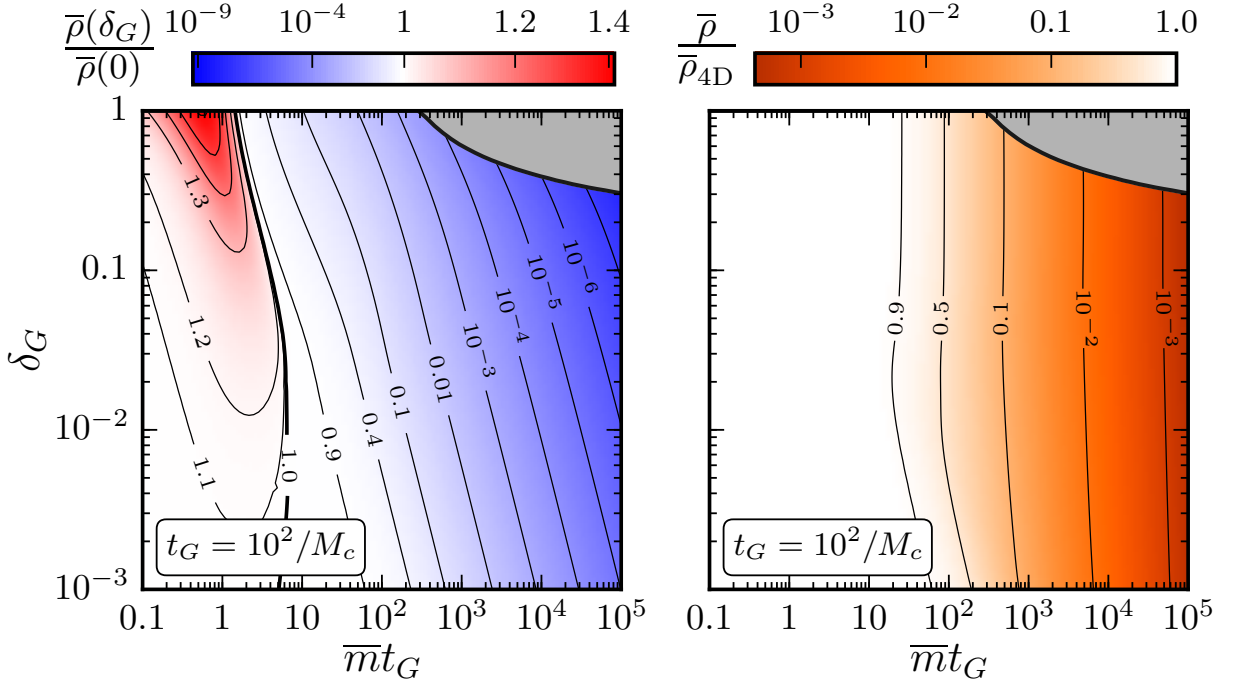


FIG. 10. The late-time energy density  $\bar{\rho}$  of the full KK tower, plotted in the  $(\bar{m}t_G, \delta_G)$  plane for  $t_G = 10^2/M_c$ . The left and right panels show contours of  $\bar{\rho}/\bar{\rho}(\delta_G = 0)$  and  $\bar{\rho}/\bar{\rho}_{4D}$ , respectively.

We can also deduce approximate scaling laws from these expressions. For  $\bar{m}/M_c \gg 1$ , we find that Eq. (6.1) approximately reduces to

$$\frac{\bar{\rho}(\delta_G)}{\bar{\rho}(0)} \sim \frac{1}{\bar{m}t_G\delta_G} \left( \frac{M_c}{\bar{m}} \right) \quad (6.3)$$

which is a factor of  $M_c/\bar{m}$  greater than the corresponding expression we observed in Eq. (3.5) for the 4D case with  $N = 1$ . Thus the presence of an entire tower of KK states suppresses what would otherwise have been the late-time energy density of the zero mode alone by an additional factor of  $M_c/\bar{m}$ . Likewise, for  $\bar{m}/M_c \gg 1$ , we observe from Eq. (6.2) that

$$\frac{\bar{\rho}}{\bar{\rho}_{4D}} \sim \frac{M_c}{\bar{m}}. \quad (6.4)$$

Thus, combining these results for  $\bar{m}/M_c \gg 1$ , we find that

$$\frac{\bar{\rho}(\delta_G)}{\bar{\rho}(0)} \sim \frac{\bar{\rho}(\delta_G)}{\bar{\rho}_{4D}(\delta_G)} \cdot \frac{\bar{\rho}_{4D}(\delta_G)}{\bar{\rho}_{4D}(0)} \quad (6.5)$$

from which we deduce that

$$\bar{\rho}(0) \sim \bar{\rho}_{4D}(0). \quad (6.6)$$

This in turn requires that there exist a constant  $c$  for which

$$\lim_{\delta_G \rightarrow 0} \left( \frac{\bar{\rho}}{\bar{\rho}_{4D}} \right) \approx c, \quad (6.7)$$

and indeed this last relation is true for  $c = 1$ . According to the results shown in the right panel of Fig. 10, this relation with  $c = 1$  is manifestly true for  $\bar{m}/M_c \lesssim 1$ . However, as  $\delta_G$  approaches zero, this relation with  $c = 1$  becomes true for larger and larger values of  $\bar{m}/M_c$ . Thus, all of the scaling relations we have quoted here are self-consistent within the regions of validity claimed.

In this connection, we remark that it is not only the power-law scaling relations in Eqs. (6.3) and (6.4) which must be consistent with each other; the same must also be true of the more complete expressions such as those in Eqs. (6.1) and (6.2) from which these power-law relations are derived. However, although such self-consistent pairs of expressions exist, the specific expressions provided in Eqs. (6.1) and (6.2) do not constitute such a pair. Rather, these expressions are provided instead because they yield even greater numerical accuracy over their appropriate regions of parameter space.

As we have seen, considering the late-time energy density  $\bar{\rho}$  as a fraction of related benchmarks such as  $\bar{\rho}(\delta_G = 0)$  or  $\bar{\rho}_{4D}$  has been useful for understanding the *relative* effects of increasing  $\delta_G$  or increasing the numbers of modes. However, we also wish to understand the late-time energy densities  $\bar{\rho}$  on an *absolute* scale. Of course, these absolute magnitudes can in principle be obtained through a sequence of multiplications of previous intermediate results. For example, one possible path is given by

$$\bar{\rho} = \left( \frac{\bar{\rho}}{\bar{\rho}_{4D}} \right) \left( \frac{\bar{\rho}_{4D}}{\bar{\rho}_{4D}(\delta_G = 0)} \right) \bar{\rho}_{4D}(\delta_G = 0) \quad (6.8)$$

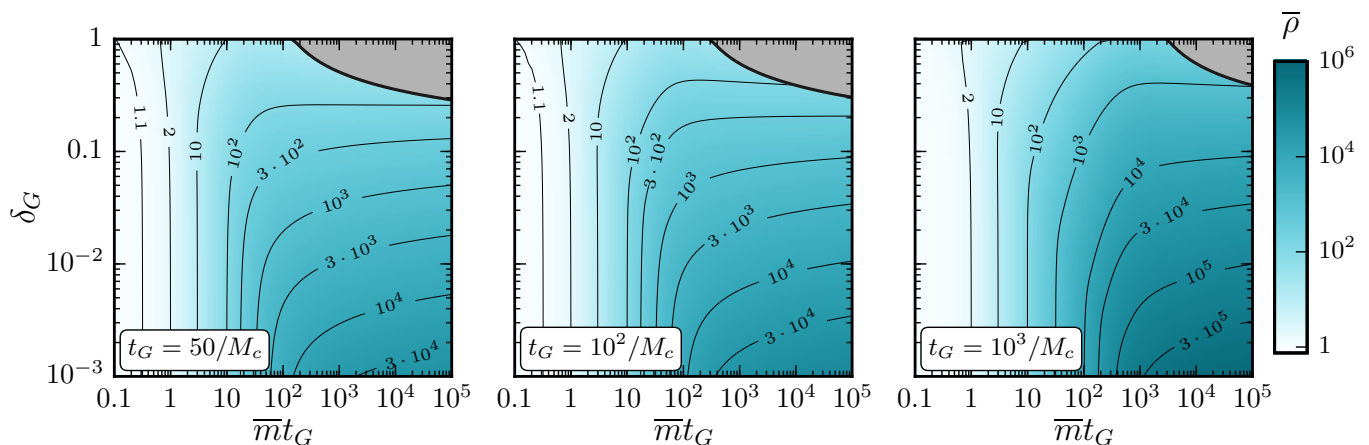


FIG. 11. The *absolute* late-time energy density  $\bar{\rho}$  in units of  $\frac{1}{2}\langle\phi\rangle^2 t^{-2}$ , plotted within the  $(\bar{m}t_G, \delta_G)$  plane for three different values of  $M_c t_G$ .

where these three different factors are indicated in the left panel of Fig. 10, the left panel of Fig. 2, and the large- $t$  behavior of Eq. (3.2) respectively. However, since each of these quantities is generally a complicated function of  $\bar{m}t_G$  and  $\delta_G$  throughout the  $(\bar{m}t_G, \delta_G)$  parameter space, it is not readily apparent what composite behavior might emerge from these individual factors. It is therefore useful to compile our intermediate results together in order to present the resulting values for  $\bar{\rho}$  as full, absolute quantities.

Our results are shown in Fig. 11 for three different values of  $t_G$ . In general, we see that taking larger values of  $\bar{m}t_G$  results in larger values of  $\bar{\rho}$ . However, we also see that taking larger values of  $\delta_G$  tends to suppress  $\bar{\rho}$ . Together, these effects conspire to produce the curved contours shown. Indeed, increasing  $t_G$  relative to  $M_c$  then tends to push these contours to the right, thereby again increasing the late-time energy density  $\bar{\rho}$  still further.

In Fig. 11 we indicated the full, absolute magnitudes of  $\bar{\rho}$  for entire our KK tower as functions of  $\bar{m}t_G$  and  $\delta_G$ . However, we are also interested in the distribution of this total energy density across the different modes of our KK tower. As we have seen throughout this paper, one measure of this distribution is the tower fraction  $\eta$  — the fraction of the total abundance which is carried by all but the most abundant mode in the tower. The late-time values of these tower fractions for the full KK tower are plotted in Fig. 12. As we see upon comparison with its finite- $N$  equivalents in Fig. 6, *passing to the infinite- $N$  limit has the effect of removing all non-monotonicities in  $\bar{\eta}$* . Indeed, we see that  $\bar{\eta}$  now increases monotonically as either  $\bar{m}t_G$  is increased or  $\delta_G$  is decreased. We stress that this is a feature which emerges only for the full KK tower with  $N = \infty$ , but which would not be true for any finite value of  $N$ . As a result, *it is the region with large  $\bar{m}t_G$  (or equivalently large  $\bar{m}/M_c$ ) and relatively small  $\delta_G$  for which the total energy density ends up distributed most broadly across the different states in the KK tower at late*

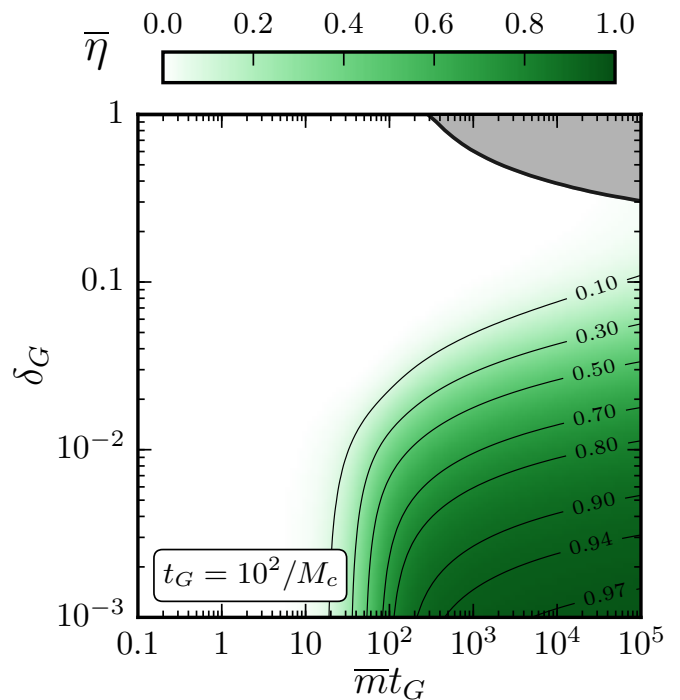


FIG. 12. The late-time tower fraction  $\bar{\eta}$  of the KK tower, plotted within the  $(\bar{m}t_G, \delta_G)$  plane for  $t_G = 10^2/M_c$ . Unlike the tower fractions illustrated in Fig. 7 for finite  $N$ , we see that the tower fraction for  $N = \infty$  is now monotonic in both  $\bar{m}t_G$  and  $\delta_G$  and approaches unity for large  $\bar{m}t_G$  and small  $\delta_G$ .

*times.*

While  $\bar{\eta}$  represents one measure of the degree to which the late-time total energy density of the KK tower is distributed across its different modes, this quantity still does not tell us how many modes are actually carrying a significant abundance. More specifically, we would like to know the shape the overall “profile” of the energy-density

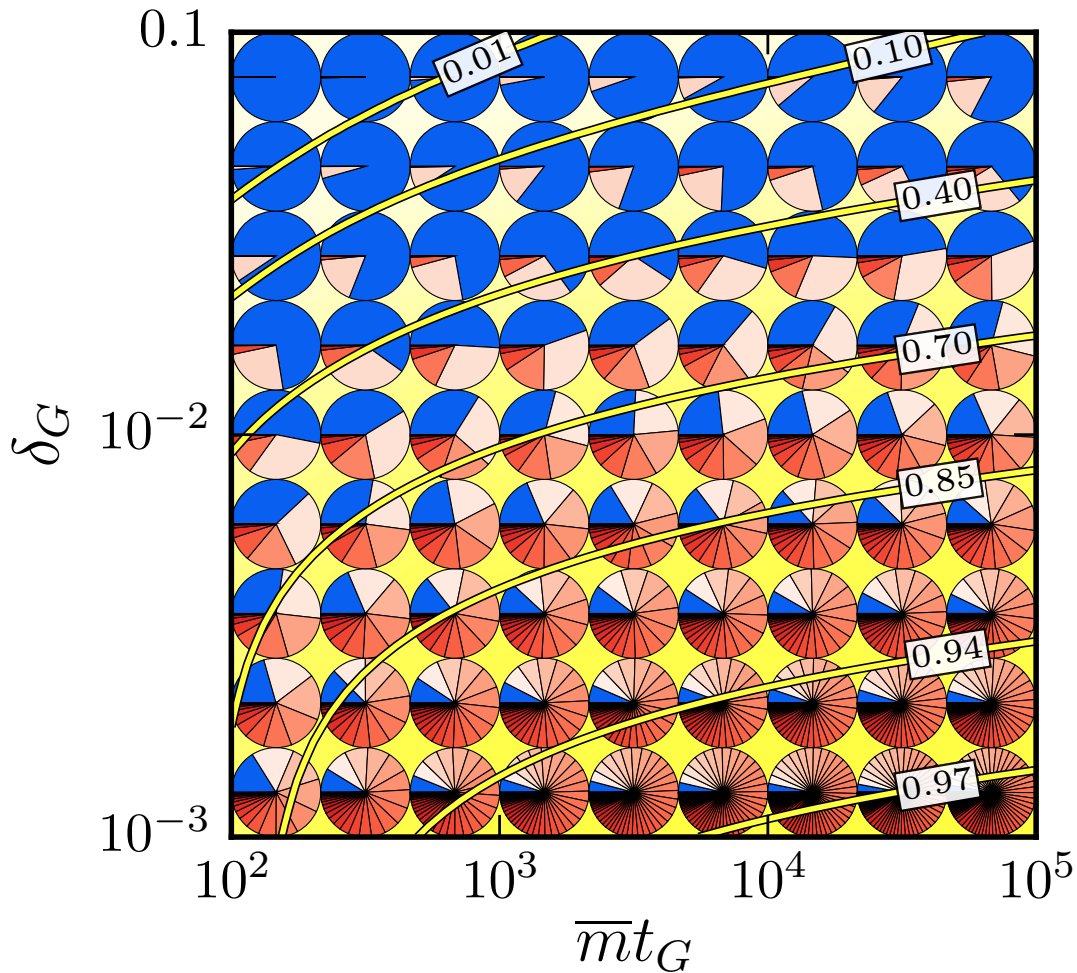


FIG. 13. A graphical representation of the distribution of the energy densities  $\bar{\rho}_\lambda$  across the entire KK tower, calculated for a square “lattice” of locations in the  $(\bar{m}t_G, \delta_G)$  plane. Each pie chart indicates how the total  $\bar{\rho}$  is distributed across the different KK modes, with the blue slices indicating the contribution associated with the lightest mode and the remaining slices (colored pink through dark red) indicating the contributions from successively heavier KK modes. The results for each pie correspond to the parameters  $(\bar{m}t_G, \delta_G)$  associated with the location of the center of the pie, and the yellow contours indicate the corresponding values of  $\bar{\eta}$ , as taken from Fig. 12. We see that the total energy density is preferentially captured by the lightest mode for larger  $\delta_G$  or smaller  $\bar{m}t_G$ , but that the total energy density is distributed more democratically across the KK tower for smaller  $\delta_G$  and larger  $\bar{m}t_G$ . Thus a wide variety of energy-density distributions across the KK tower can be realized simply by adjusting the parameters associated with the mass-generating phase transition.

distribution across the entire KK tower as a function of  $\bar{m}t_G$  and  $\delta_G$ . Towards this end, we can visualize the shape of a given energy-density distribution profile by means of a pie chart whose different pie slices illustrate how  $\bar{\rho}$  is distributed across the different KK modes. We then seek to understand how the relative slices of such pies evolve as functions of  $\bar{m}t_G$  and  $\delta_G$ .

Our results are shown in Fig. 13 for  $t_G = 10^2/M_c$ . In Fig. 13 we have focused on the non-trivial green region of Fig. 12 wherein  $\bar{\eta} > 0$ , and then superimposed a set of pie charts illustrating how the energy-density profile varies across this region. We see from this figure that the total energy density tends to be preferentially captured by the lightest mode as  $\delta_G$  increases or  $\bar{m}t_G$  decreases, but that

the total energy density tends to be more democratically distributed across the KK modes of the tower otherwise. *We see, then, that a wide variety of energy-density distributions across the KK tower are possible and can be realized simply by adjusting the parameters associated with the mass-generating phase transition.*

Finally, we can summarize the results of this section by combining our information concerning the absolute *magnitudes* of the late-time total energy density  $\bar{\rho}$ , as indicated in Fig. 11, with our information concerning the late-time *distributions* of that total energy density, as indicated in Fig. 13. To do this, we can begin with the information in Fig. 13 but then *rescale the size of each pie chart so that the area of each pie chart is proportional to*



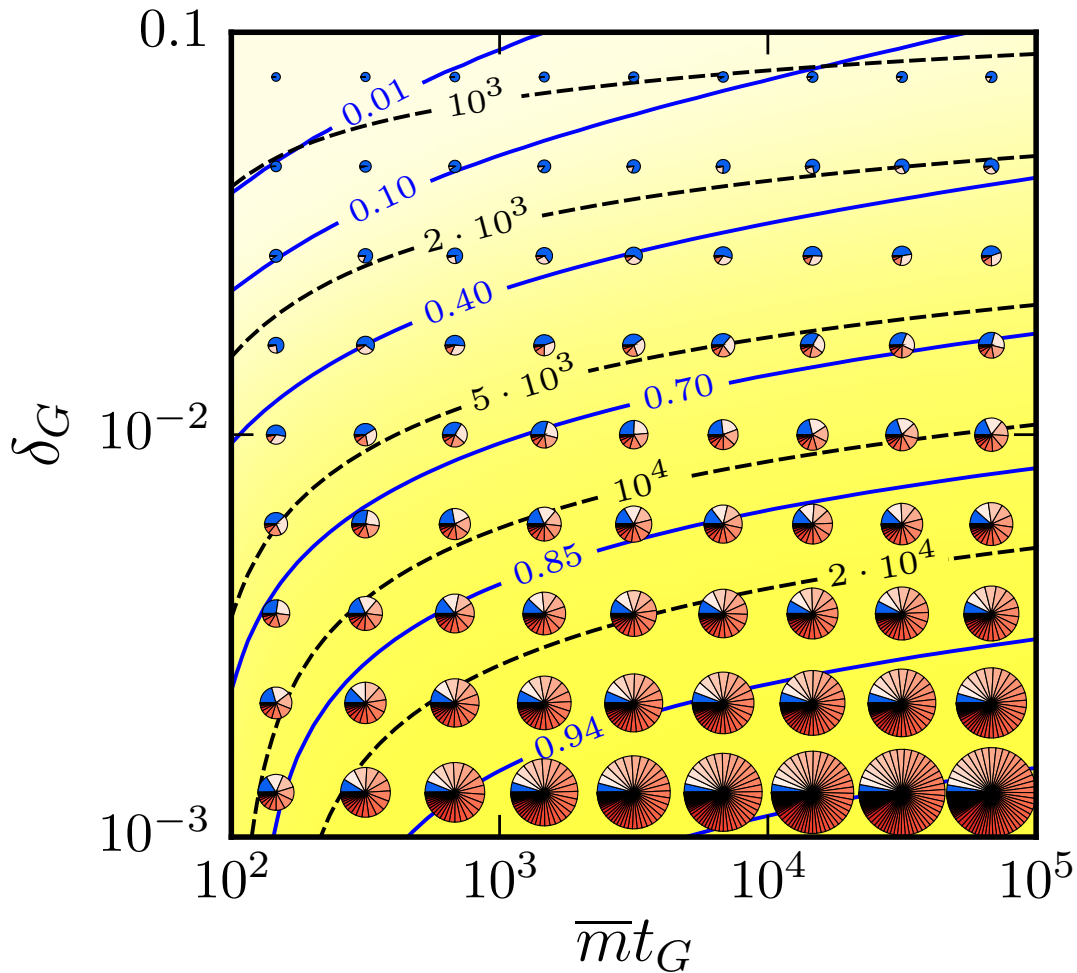


FIG. 14. A grand summary of the results of this section, combining our information concerning the absolute *magnitudes* of the total late-time energy density  $\overline{\rho}$  from Fig. 11 with our information concerning the *distribution* of that energy density from Fig. 13, all plotted within the  $(\overline{m}t_G, \delta_G)$  plane. This figure is essentially the same as Fig. 13 except that the overall areas of our pie charts have been rescaled in proportion to the magnitudes of the total late-time energy densities  $\overline{\rho}$  shown in Fig. 11. In the background we have also indicated the contours of  $\overline{\rho}$  from Fig. 11 (dashed black lines) as well as the contours of  $\overline{\eta}$  from Fig. 12 (solid blue lines). We see that there is a non-trivial *correlation* between the overall magnitude of  $\overline{\rho}$  and the distribution of that energy density, with larger energy densities distributed more democratically across the KK tower and smaller energy densities captured more and more preferentially by the lightest KK mode. Both features are nevertheless extremely sensitive to the parameters governing the mass-generating phase transition, with the former behavior dominating for smaller  $\delta_G$  and larger  $\overline{m}t_G$  and the latter dominating for larger  $\delta_G$  and smaller  $\overline{m}t_G$ .

the total energy density  $\overline{\rho}$ . The result is shown in Fig. 14.

One important lesson that emerges from Fig. 14 is that there is a non-trivial correlation between the overall *magnitude* of  $\overline{\rho}$  and the *distribution* of that energy density, with larger energy densities distributed more democratically across the KK tower and smaller energy densities captured more and more preferentially by the lightest KK mode. The results in Fig. 14 allow us to see rather dramatically the effects of our mass-generating phase transition on the eventual late-time energy configuration of our KK tower. For any fixed  $\overline{m}t_G$ , we see that increasing the phase-transition timescale  $\delta_G$  suppresses the energy density that remains in the massive KK modes, caus-

ing the lighter modes to assume an increasing fractional share of the total energy density. Yet, at the same time, increasing  $\delta_G$  suppresses the total energy density that is ultimately pumped into the KK tower by the phase transition. Likewise, for any  $\delta_G$ , we see that increasing  $\overline{m}t_G$  increases the total energy pumped into the system by the phase transition while simultaneously causing this energy density to be more democratically distributed. *Thus, merely by choosing appropriate values of  $\overline{m}t_G$  and  $\delta_G$ , it is possible to adjust the total absolute energy density remaining in the KK tower at late times to any value one might select for phenomenological purposes while simultaneously retaining the ability to adjust the distribution of*

that energy density across the different KK modes. This, then, is the power of the mass-generating phase transition and the influence of its associated timescale.

## VII. EXAMPLE: AXION IN THE BULK

Until this point, we have maintained generality by considering a higher-dimensional field  $\Phi$  and specifying little more about this field than that it is a scalar. Likewise, we have assumed little more about our phase transition than that it generates masses in a time-dependent way. However, in order to explore one possible set of phenomenological implications of our results, we shall now apply our machinery to the case in which  $\Phi$  is an axion-like particle and in which our phase transition on the brane is one in which instanton-like effects give mass to that axion.

We begin by considering the setup described in Refs. [24, 25], which is itself a generalization of an earlier framework considered in Ref. [22]. Specifically, we consider the same five-dimensional geometry as discussed in previous sections and henceforth take

$$M_c = 4.49 \times 10^{-12} \text{ GeV} \quad (7.1)$$

as our compactification scale. This value of  $M_c$  corresponds to  $R \approx 44 \mu\text{m}$ , which is the largest flat extra dimension allowed according to data from torsion-balance experiments [38]. Within the bulk of this extra dimension we shall consider a (pseudo-)scalar field  $\Phi$  which is a straightforward generalization of the traditional QCD axion [1, 3, 4]. In particular, we shall take  $\Phi$  to be the Nambu-Goldstone boson associated with a global chiral Peccei-Quinn-like  $U(1)_X$  symmetry which is spontaneously broken at some scale  $f_X$ . This  $U(1)_X$  symmetry is assumed anomalous, and for a non-Abelian gauge group  $G$  on the brane with coupling  $g$  and field strength  $\mathcal{G}_{\mu\nu}$ , this anomaly therefore generates a topological brane term of the form

$$\mathcal{L}_{\text{brane}} \rightarrow \mathcal{L}_{\text{brane}} + \frac{\mathcal{C}g^2}{32\pi^2} \frac{\Phi}{f_X^{3/2}} \text{Tr } \mathcal{G}_{\mu\nu} \tilde{\mathcal{G}}^{\mu\nu} \quad (7.2)$$

where  $\mathcal{C}$  is a model-dependent constant. While this term has no effect on the classical equations of motion, it affects the vacuum structure of the theory. As the universe cools and reaches  $T \sim \Lambda_G$ , where  $\Lambda_G$  is the confinement scale associated with the group  $G$ , instanton effects on the brane explicitly break the  $U(1)_X$  axion shift symmetry that prevents the axion from acquiring a mass. As a result, a small temperature-dependent axion mass  $m_X(T)$  is generated on the brane. In general, we shall model the time dependence of this mass exactly as in previous sections, as resulting from a phase transition occurring at a time  $t_G$  with a width  $\delta_G$ . In this connection we note that our adoption of an LTR cosmology, as discussed in Sect. II, implies that this phase transition takes place during an inflaton-dominated (and thus matter-dominated) epoch. The corresponding time/temperature

relationship then yields the result

$$t_G = \sqrt{\frac{45g_*(T_{\text{RH}})}{2\pi^2}} \frac{T_{\text{RH}}^2 M_p}{g_*(\Lambda_G) \Lambda_G^4} \quad (7.3)$$

where  $T_{\text{RH}} \sim \mathcal{O}(\text{MeV}) < \Lambda_G$  is the reheating temperature, where  $g_*(T)$  is the effective number of relativistic degrees of freedom at temperature  $T$ , and where  $M_p \equiv 1/\sqrt{8\pi G}$  is the reduced Planck mass. For concreteness we shall take  $T_{\text{RH}} = 30 \text{ MeV}$  in what follows. Finally, at late times, our phase transition leaves our axion-like field with a brane mass given by

$$\bar{m}_X^2 \equiv \frac{\mathcal{C}^2 g^2 \Lambda_G^4}{32\pi^2 \hat{f}_X^2} \quad (7.4)$$

where we have defined the effective four-dimensional  $U(1)_X$ -breaking scale  $\hat{f}_X \equiv \sqrt{2\pi R} f_X^3$ .

The above setup defines our five-dimensional axion theory. Compactifying this theory via KK reduction then yields an effective four-dimensional theory consisting of a KK tower of axion modes  $\phi_k$  whose mass matrix takes exactly the form given in Eq. (2.6), with  $m(t)$  now identified as  $m_X(t)$ . Thus, we see that our axion model is nothing but a special case of the model we have already considered thus far — the special case in which we identify  $\bar{m}$  as  $\bar{m}_X$  and identify  $t_G$  as the cosmological time corresponding to the temperature  $T \sim \Lambda_G$ , as in Eq. (7.3).

In previous sections, we studied the behavior of our general KK system as a function of the four parameters  $\{\bar{m}, M_c, t_G, \delta_G\}$ . For our axion theory, by contrast, we see that  $\bar{m} \rightarrow \bar{m}_X$ , and moreover we see that both  $\bar{m}_X$  and  $t_G$  are themselves related to the more fundamental parameters  $\Lambda_G$  and  $\hat{f}_X$  through Eqs. (7.4) and (7.3) respectively. Thus, we shall henceforth consider our axion theory to be parametrized by  $\{\Lambda_G, \hat{f}_X, M_c, \delta_G\}$ .

In four dimensions, the methods used to estimate the late-time abundance of a given axion field typically fall into one of two classes examined in Sect. III: the adiabatic approximation or the abrupt approximation. As we have seen, the former only applies when the mass is generated sufficiently slowly during field oscillations, with  $\dot{m} \ll m^2$ , while the latter applies only for very small  $\delta_G$  (such that the phase-transition width  $\Delta_G$  is much smaller than the timescale of field oscillations) or for situations in which  $t_\zeta \gg t_G$  (so that the phase transition occurs while the field is still overdamped and essentially frozen). However, as we have seen in previous sections, these approximations break down in relatively large regions of parameter space. We should also expect deviations from our standard expectations in the case of an infinite KK tower of axion modes. For example, the virialization condition that underpins the adiabatic approximation now becomes  $\lambda_0 \ll \lambda_0^2$ , and  $\lambda_0$  can be much smaller than  $m_X$  [22]. Likewise, there is always some subset of modes in the KK tower for which  $t_\zeta^{(\lambda)} \lesssim t_G$ . Such modes are therefore necessarily affected by the time-dependence of the phase transition.

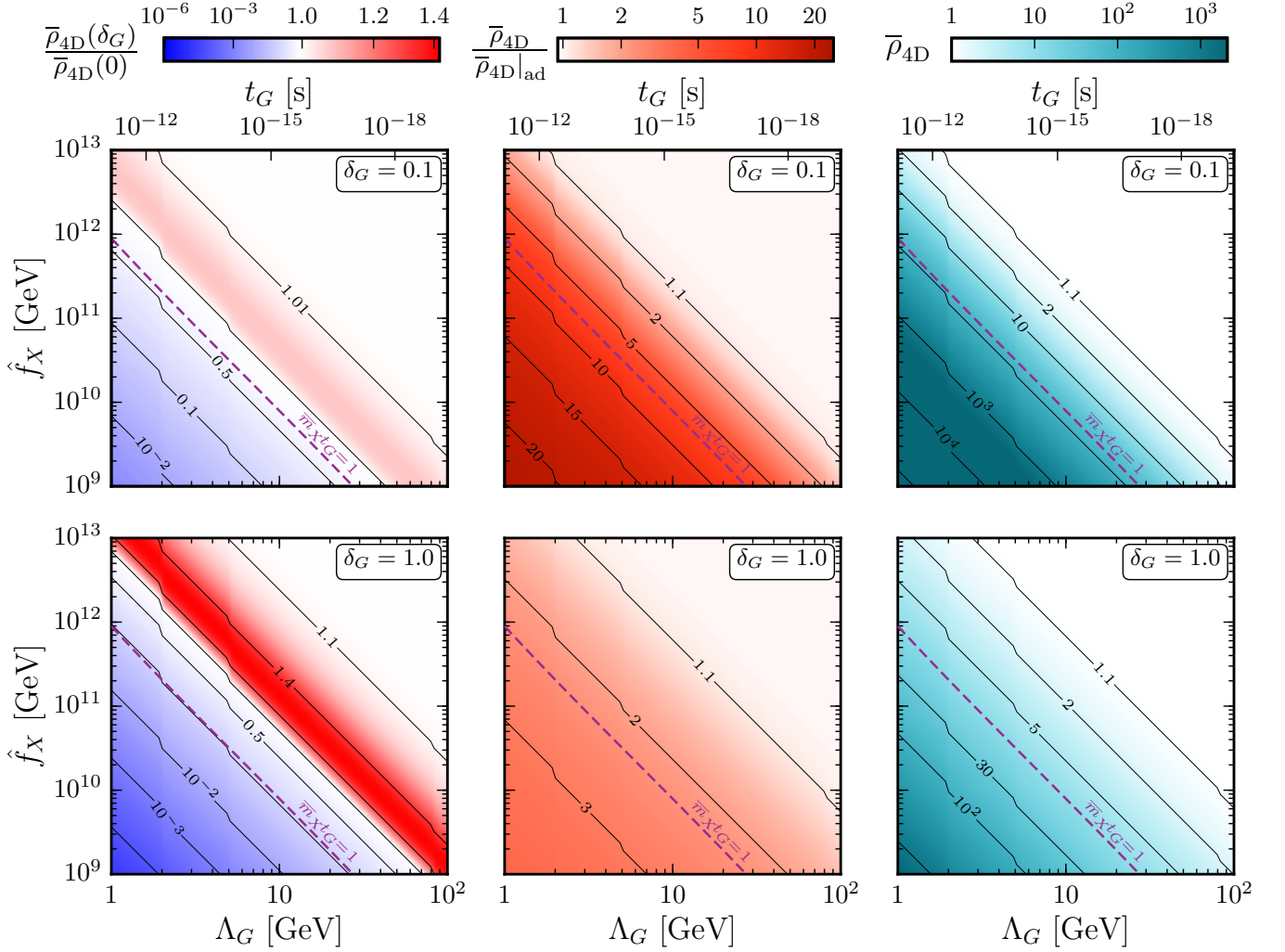


FIG. 15. The late-time energy density  $\bar{\rho}_{4D}$  of our generalized axion field in the 4D limit, plotted within the  $(\Lambda_G, \hat{f}_X)$  plane for  $\delta_G = 0.1$  (top row) and  $\delta_G = 1.0$  (bottom row). Note that the horizontal  $\Lambda_G$  axis (as shown along the bottom of each panel) is equivalently a  $t_G$  axis (as shown along the top). The panels in the left and middle columns plot  $\bar{\rho}$  as fractions of the abrupt and adiabatic approximations  $\bar{\rho}_{4D}(\delta_G = 0)$  and  $\bar{\rho}_{4D}|_{\text{ad}}$ , respectively, while the panels in the right column plot the absolute magnitude of  $\bar{\rho}_{4D}$  in units of  $\frac{1}{2}(\phi)^2 t^{-2}$ . Also shown in each panel is a purple dashed line indicating the contour along which  $\bar{m}_X t_G = 1$ .

In this section, we shall therefore present exact results for the late-time energy densities of our axion fields. We shall do this both for the four-dimensional  $N = 1$  case as well as the infinite- $N$  case of our full KK axion tower. As discussed above, we shall take our axion parameter space to be parametrized by  $\{\Lambda_G, \hat{f}_X, M_c, \delta_G\}$ . However, we stress that the plots to be presented in this section are not merely translations of our previous plots into these new variables. First, we have extended our range of interest within this parameter space into those regions of specific interest for axion physics. Second, we shall now regard  $\Lambda_G$  and  $\hat{f}_X$  as the fundamental axion parameters relative to which we wish to consider continuous variations. In other words, we shall plot our the late-time energy densities  $\bar{\rho}$  as functions of  $\Lambda_G$  and  $\hat{f}_X$  within the  $(\Lambda_G, \hat{f}_X)$  plane, choosing only discrete representative choices for

$\delta_G$ . This too is different than what was done in previous sections, and thus represents a different, independent slice through our four-dimensional parameter space.

We begin, as in Sect. III, by considering the four-dimensional  $N = 1$  limit. In this case, we find the results shown in Fig. 15. We observe from the panels in the left and center columns of Fig. 15 that there are distinct regions of parameter space in which the abrupt and adiabatic approximations fail to model the true late-time energy density, with the adiabatic approximation consistently underestimating the true energy density and the abrupt approximation either under- or overestimating the true energy density, in some cases by many orders of magnitude. We also see that increasing either the confinement scale  $\Lambda_G$  or the  $U(1)_X$  symmetry-breaking scale  $\hat{f}_X$  generally decreases the late-time energy density of our

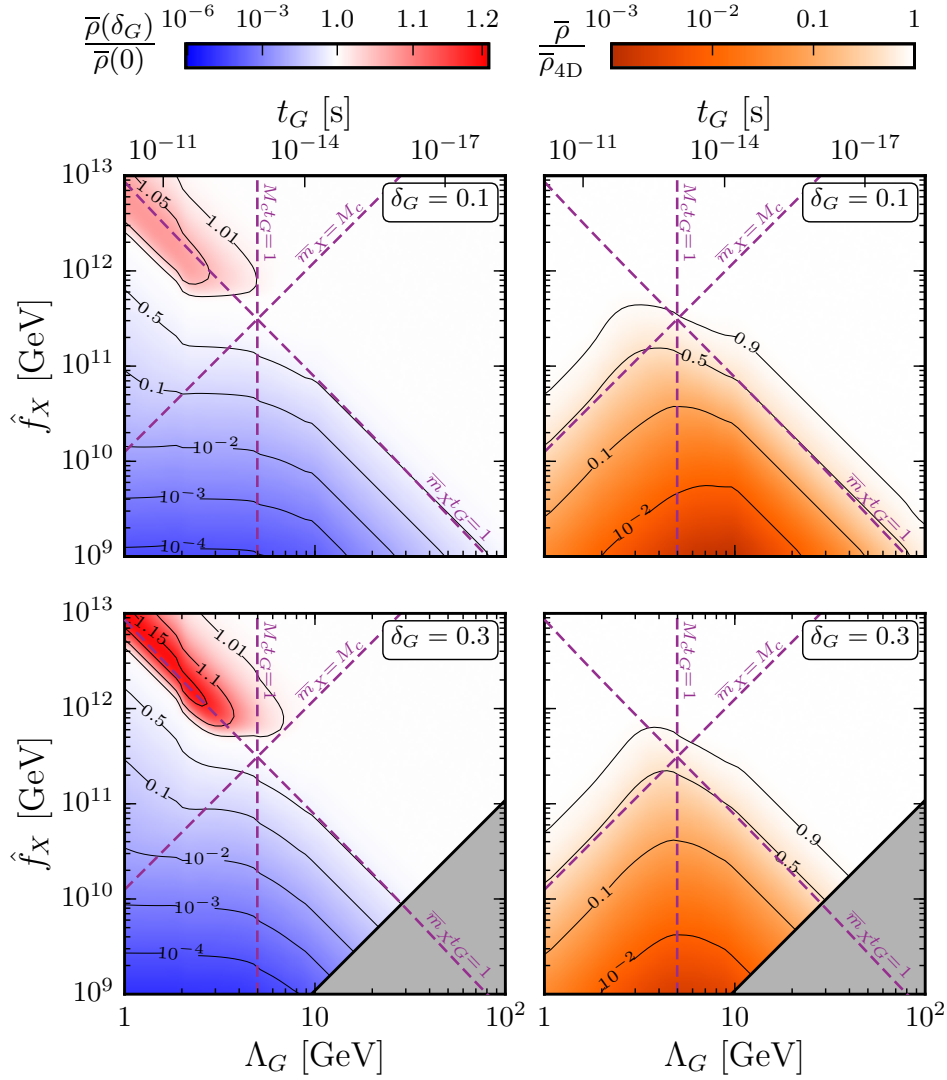


FIG. 16. The total late-time energy density  $\bar{\rho}$  of our generalized axion KK tower, plotted as fractions of  $\bar{\rho}(\delta_G = 0)$  (left column) or  $\bar{\rho}_{4D}$  (right column) within the  $(\Lambda_G, \hat{f}_X)$  plane for  $\delta_G = 0.1$  (top row) and  $\delta_G = 0.3$  (bottom row). As in Fig. 15, the  $\Lambda_G$  axis is shown along the bottom of each panel while the equivalent  $t_G$  axis is shown along the top. Also shown in each panel are three purple dashed lines indicating the contours along which  $\bar{m}_X t_G = 1$ ,  $\bar{m}_X = M_c$ , or  $M_c t_G = 1$ . As with other figures in this paper, the gray regions are excluded for the reasons discussed in the paragraph below Eq. (2.12).

axion field. Increasing the width  $\delta_G$  of our axion-induced phase transition also has the same effect. Indeed, we see from the relatively straight contours in Fig. 15 that the absolute magnitude of the late-time energy density scales approximately as

$$\bar{\rho}_{4D} \sim 1/(\Lambda_G^4 \hat{f}_X^2), \quad (7.5)$$

where the constant of proportionality is a non-trivial function of  $\delta_G$ . This scaling behavior is of course consistent with the analogous result in Eq. (3.9). Finally, we note that all of the contour lines in Fig. 15 experience slight “ripples” at  $\Lambda_G \approx 2$  GeV and 5 GeV. These ripples are physical, and correspond to the energy scales  $\Lambda_G$  at which there are changes in the number  $g_*(\Lambda_G)$  of relativistic degrees of freedom (the former corresponding

to the threshold for the charm quark and tau lepton, and the latter corresponding to the threshold for the bottom quark).

We now turn to the case in which a full KK tower of axion modes experiences the instanton-induced phase transition. In this case, our results are plotted in Figs. 16 through 18. In Fig. 16 we have plotted the values of the late-time total energy density  $\bar{\rho}$  of the KK tower relative to our usual benchmarks  $\bar{\rho}(\delta_G = 0)$  and  $\bar{\rho}_{4D}$ . Once again, we see that the introduction of a non-zero width  $\delta_G$  for our instanton-induced phase transition leads to either enhancements or suppressions in  $\bar{\rho}$ , depending on the specific region of parameter space. Moreover, we see that increasing  $\delta_G$  only makes these enhancements or suppressions more severe. By contrast, turning to  $\bar{\rho}/\bar{\rho}_{4D}$ , we see



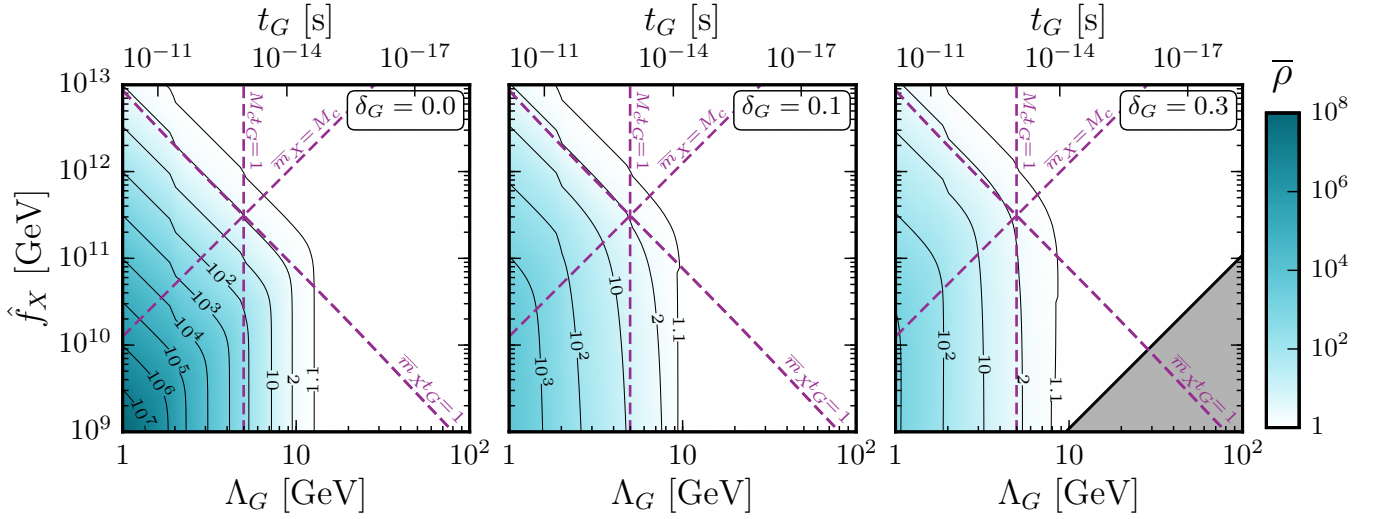


FIG. 17. The absolute magnitude of the total late-time energy density  $\bar{\rho}$  of our generalized axion KK tower, plotted in units of  $\frac{1}{2}\langle\phi\rangle^2 t^{-2}$  within the  $(\Lambda_G, \hat{f}_X)$  plane for  $\delta_G = 0$  (left panel),  $\delta_G = 0.1$  (middle panel), and  $\delta_G = 0.3$  (right panel).

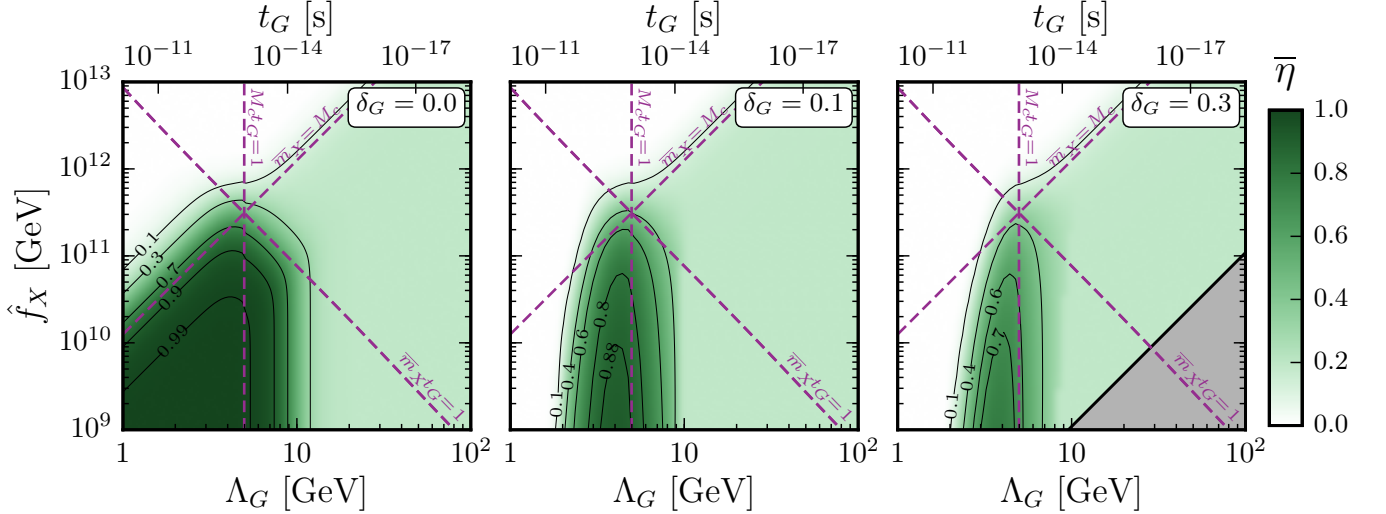


FIG. 18. The late-time tower fraction  $\bar{\eta}$  of our generalized axion KK tower, plotted within the  $(\Lambda_G, \hat{f}_X)$  plane for  $\delta_G = 0$  (left panel),  $\delta_G = 0.1$  (middle panel), and  $\delta_G = 0.3$  (right panel).

the introduction of the extra KK modes in the tower only suppresses  $\bar{\rho}$  by an amount that grows *less* severe for increasing  $\delta_G$ . In all cases, however, these suppressions tend to be more pronounced for smaller  $\Lambda_G$  and smaller  $\hat{f}_X$  than they are in other regions of parameter space. It is worth noting that for smaller  $\Lambda_G$  (but  $\bar{m}_X \gg M_c$ ), we see a scaling behavior of the form

$$\frac{\bar{\rho}}{\bar{\rho}_{4D}} \sim \frac{\hat{f}_X}{\Lambda_G^2}. \quad (7.6)$$

However, as  $\Lambda_G$  increases (and thus  $t_G$  decreases), this scaling behavior eventually breaks down and the behavior of  $\bar{\rho}/\bar{\rho}_{4D}$  is increasingly determined solely by the behavior

of the denominator  $\bar{\rho}_{4D}$ , with contours of constant  $\bar{m}_X t_G$ . Otherwise, outside the  $\bar{m}_X \gtrsim M_c$  and  $\bar{m}_X t_G \gtrsim 1$  region, the energy density at late times is very similar to that in the 4D limit.

It is also instructive to compare our KK results for  $\bar{\rho}/\bar{\rho}(\delta_G = 0)$  along the left column of Fig. 16 with the analogous 4D results along the left column of Fig. 15. For the full KK tower, we no longer find contours of constant  $(\bar{m}_X t_G)^2$ ; instead we find a region exhibiting contours with approximately constant  $\hat{f}_X$ . Likewise, the enhancement region that we found in the 4D limit spanned the entire  $\{\Lambda_G, \hat{f}_X\}$  parameter space for  $\bar{m}_X t_G \sim 1$ , whereas this region for the KK tower exists only for  $\bar{m}_X \lesssim M_c$ .

Next, we turn to Fig. 17 where we plot the absolute magnitude of the total late-time energy density of the KK axion tower in units of  $\frac{1}{2}\langle\phi\rangle^2 t^{-2}$ . To help understand the features of these plots and how they evolve as a function of  $\delta_G$ , we have included a panel with  $\delta_G = 0$  whose features can be understood directly via the abrupt approximation. Indeed, as expected, we see that all  $\bar{\rho}$  contours in the  $\delta_G = 0$  case are contours of either constant  $\bar{m}_X t_G$ , constant  $\bar{m}_X/M_c$ , or constant  $M_c t_G$ . The subsequent panels then illustrate how these contours deform as the width  $\delta_G$  of our phase transition increases.

Likewise, in Fig. 18, we plot the late-time tower fraction  $\bar{\eta}$  of our KK axion tower. Once again, we see a consistent picture emerging as a function of  $\delta_G$ . Indeed, just as for  $\bar{\rho}$  in Fig. 17, we see that all  $\bar{\eta}$  contours for  $\delta_G = 0$  are contours of either constant  $\bar{m}_X t_G$ , constant  $\bar{m}_X/M_c$ , or constant  $M_c t_G$ , with the subsequent panels once again illustrating how these contours deform as  $\delta_G$  increases. From the left panel of Fig. 18 we see that when the phase transition is abrupt, the total energy density of the tower is distributed amongst a significant number of KK modes in the small- $\Lambda_G$ , small- $\hat{f}_X$  corner of parameter space. However, as our mass-generating phase transition unfolds over a longer period of time, the energy contributions from the higher modes are suppressed and  $\bar{\eta}$  begins to fall.

One interesting feature apparent in Fig. 18 is that the value of  $\bar{\eta}$  is non-monotonic as a function of  $\Lambda_G$ , first increasing and reaching a maximum near  $\Lambda_G \approx 3$  GeV before decreasing again. This can be understood as follows. The vanishing of  $\bar{\eta}$  for  $\bar{m}_X \ll M_c$  is understood from the distribution of initial abundances as described in Fig. 4. Indeed, in this region, nearly all of the abundance of the KK tower is contributed by the lowest KK mode because very little mixing is generated in the phase transition. By contrast, the decline in  $\bar{\eta}$  which occurs as  $\Lambda_G$  increases (or equivalently as  $t_G$  decreases) can be understood as corresponding to our entrance into what in Refs. [23–25] was called the “staggered” regime wherein the heavier KK modes are oscillating (and thus already dissipating their energy density) as soon as our phase transition occurs, whereas the lighter KK modes remain overdamped for a long time after  $t_G$ . This then results in a total abundance composed primarily of contributions from those lighter modes.

Comparing the results in Figs. 17 and 18, we see that the regions of parameter space which produce the largest total energy densities  $\bar{\rho}$  almost coincide exactly with the regions that produce the largest tower fractions  $\bar{\eta}$ . Indeed, both regions have very small  $\hat{f}_X$ , and the only difference is that the former region has small  $\Lambda_G$  while the latter region has  $\Lambda_G \approx 3$  GeV. At first glance, this difference may appear to violate the claims made in connection with Fig. 14, namely that these two regions should coincide completely. However, the correlation observed in connection with Fig. 14 holds when  $t_G$  is held fixed. By contrast, the results in Figs. 17 and 18 are generated with  $t_G$  implicitly varying throughout the parameter

space shown.

Having focused in this section on the specific situation in which our  $\Phi$  field is an axion, one possible next step would be to place phenomenological bounds on the parameter spaces we have considered. Such bounds would in principle mirror those which are normally applied to the case of a traditional QCD axion, and come from a variety of considerations including supernova cooling, black hole superradiance, overclosure constraints, dark-matter and dark-energy constraints, traditional axion searches (such as light shining through walls), *etc.* Within the context of the abrupt ( $\delta_G = 0$ ) limit, such bounds on KK axion towers are discussed in detail in Ref. [25]. Although the determination of such bounds for general  $\delta_G$  is beyond the scope of this paper, the results we have obtained here concerning the late-time energy densities of these axion systems should play a critical role in helping to determine exactly where these bounds lie for general  $\delta_G$ , and the extent to which the suppressions and enhancements we have observed translate into a loosening or strengthening of those bounds beyond traditional expectations.

## VIII. DISCUSSION AND CONCLUSIONS

In this paper we have investigated the effects of dynamical mass generation on the cosmological abundances of the Kaluza-Klein modes associated with a bulk scalar field. In particular, we have examined the non-trivial case in which a phase transition localized on a brane leads to time-dependent masses and mixings among these KK modes. We have found that both the total energy density of the full KK tower and the distribution of that energy density across the individual KK modes are extremely sensitive to the details of the phase transition. As a result, within different regions of model parameter space, these abundances can be significantly enhanced or suppressed relative to standard expectations — sometimes by many orders of magnitude. We have also derived a variety of approximate scaling behaviors and analytic expressions for the energy densities of the KK modes as functions of the relevant model parameters. In order to illustrate the potentially significant impact that these effects can have on the late-time abundances of our scalars within the context of a concrete model, we have also applied our general results to the case of a bulk axion/axion-like field. Finally, as a by-product of our analysis, we have also developed an alternate “UV-based” effective truncation of KK theories which is physically different from the more traditional “IR-based” truncation commonly employed in the literature, yet yields the same higher-dimensional theory as the truncation is lifted.

Depending on the identity of the scalar field in question, our results can have a variety of phenomenological implications. For example, in the case in which our bulk scalar is an axion or axion-like field, one can easily imagine a number of phenomenological consequences. Note

that in general, cosmological abundances in this paper have been generated through a two-step process: the assumption of a non-zero VEV for one or more modes in the KK tower followed by a mass-generating phase transition. As such, given the specific form of the initial conditions we have adopted in Eq. (2.13), the method of abundance generation we have studied in this paper is tantamount to misalignment production. However, misalignment production is not the only mechanism through which a population of axion-like particles can be produced in the early universe. For example, spontaneous breaking of the global  $U(1)_X$  symmetry of Sect. VII can lead to the formation of a network of cosmic strings and other topological defects [39]. If this breaking occurs before cosmic inflation, these defects are simply inflated away. By contrast, if the breaking of  $U(1)_X$  occurs after inflation, these defects retain a non-negligible energy density until late times, and their decays can therefore generate a potentially significant contribution to the relic abundance of the corresponding axion-like particles. Indeed, this topic has been studied in detail for the specific case of a QCD axion [40–43], but in principle applies to other axion-like particles as well.

These considerations are important because the phase-space distribution of a population of axions or axion-like particles produced via the decays of topological defects is significantly different from that generated via misalignment production [42–44]. Thus, in cases in which the misalignment contribution to the overall late-time axion abundance is suppressed by the time-dependent masses and mixings we have discussed here, the phase-space distribution of relic axions can be significantly altered — especially if the contribution from topological defects ends up dominating the total axion abundance. Moreover, the suppression of the misalignment contribution to this overall axion abundance can also serve to weaken the overclosure bound on the axion-decay constant, and thus could potentially enlarge the allowed region of parameter space for the QCD axion.

Our results concerning the effects of a mass-generating phase transition can also have significant implications for other new-physics scenarios. For example, our results may provide a way of mitigating the cosmological moduli problem which arises in supergravity [45] and in string theory [46–48]. Indeed, such theories generically predict large numbers of neutral scalar fields — so-called moduli — with flat potentials, long lifetimes, and large (and even Planck-scale) VEVs. On the one hand, a number of phenomenological considerations imply that some mechanism must exist through which a potential is generated for these moduli, rendering them massive. On the other hand, once these fields acquire masses, they can potentially overclose the universe or precipitate an unacceptably late period of reheating. A suppression of the collective energy density of such moduli due to time-dependent mixing effects of the sort we have discussed here could potentially provide a way of addressing these issues.

Our results also have implications within the context of the Dynamical Dark Matter (DDM) framework [23, 24], an alternative framework for dark-matter physics in which a potentially vast ensemble of unstable particles contribute to the present-day dark-matter abundance and in which phenomenological constraints on the dark sector are satisfied through a balancing between constituent decay widths and cosmological abundances across the ensemble. Dark-matter ensembles with these properties emerge naturally in a variety of contexts [23, 24, 49–52], and detection strategies for such ensembles are discussed in Refs. [53–59]. Indeed, it has been shown that the KK modes associated with a bulk axion-like field which receives its abundance via misalignment production constitute a viable DDM ensemble [24, 25]. The results we have obtained here are thus directly applicable to DDM ensembles of this sort and lead to a suppression of the overall relic abundance of the ensemble for large  $\delta_G$  relative to the relic abundance which arises for the abrupt case considered in Refs. [24, 25]. This suppression can potentially widen the phenomenologically allowed parameter space of such DDM models. Moreover, we also note from the results in Fig. 14 that there exists a correlation between the overall magnitude of the late-time energy density of the KK tower and the degree to which its distribution across the different KK modes is particularly “DDM-like” (*i.e.*, shared non-trivially across many different KK modes), with larger total abundances tending to correlate with increased DDM-like behavior at late times. Thus, we see that we can control the degree to which our ensemble of KK states is truly DDM-like at late times simply by adjusting phenomenological parameters such as  $\overline{m}$  and  $\delta_G$  associated with our mass-generating phase transition.

The suppression of late-time scalar abundances due to time-dependent masses and mixings also has potentially important implications for a broad range of additional scenarios involving weakly-coupled scalar particles which receive a non-negligible contribution to their relic abundances from non-thermal mass-generating phase transitions of the sort we have discussed here. The reason is that in such scenarios, a non-negligible population of these particles can also be produced thermally from scattering processes involving SM particles in the radiation bath. This production mechanism is often referred to as “freeze-in” [60], and it also gives rise to a population of particles whose phase-space distribution differs significantly from that of the population generated by non-thermal mass-generating phase transitions. For the QCD axion, the freeze-in contribution to the total relic abundance is typically quite small [61–63] compared to the contributions from other sources, such as misalignment production and cosmic-string and domain-wall decay. By contrast, for other exotic scalars, the freeze-in contribution can be significant. Thus, in scenarios in which both misalignment production and freeze-in production are naïvely expected to generate comparable contributions to the overall abundance of a particular weakly-coupled

scalar particle, a suppression of the former contribution due to time-dependent mixing could both modify over-closure bounds and alter the expected phase-space distribution of the relic scalar population.

In this paper we have focused on the contribution to the total abundance of a collection of KK scalar modes that arises due to a time-dependent mass-generating phase transition. In so doing, however, we have disregarded the effects of the quantum fluctuations that arise for these fields during the inflationary epoch. In general, fluctuations in the long-wavelength modes of light fields — and, in particular, those modes whose wavelengths exceed the Hubble length during that epoch — behave like vacuum energy until after inflation ends. Thus, the energy density in these fluctuations survives inflation and yields an additional contribution to the abundance of any field with mass  $\lambda_k \lesssim H_I$ , where  $H_I$  is the value of the Hubble parameter during inflation. This additional contribution depends sensitively on the parameters of the inflationary model (for a review, see, *e.g.*, Ref. [64]) and in particular on  $H_I$  itself. In Ref. [25], it was shown that for a KK tower of axion-like fields, the contribution to the relic abundance from vacuum misalignment dominates over this additional contribution from fluctuations during inflation for sufficiently small  $H_I$ . However, we note that in general, this contribution exists and for higher-scale inflationary models may have a significant impact on the overall relic abundance of the KK tower.

In the course of our analysis in this paper, we also derived results for truncated KK towers consisting of only  $N$  modes, where  $N < \infty$ . In so doing, we presented the results of this finite- $N$  case merely as a stepping stone on the way towards understanding the properties of the full KK tower that emerges in the  $N \rightarrow \infty$  limit. However, the results of our finite- $N$  analysis are also interesting in their own right. Indeed, the mass-squared matrix for a tower of  $N$  modes is similar to the mass matrix which emerges in certain “moose” [65] or “quiver” [66] gauge theories — theories which also contain only a finite number of modes yet which yield a deconstructed extra spacetime dimension in the  $N \rightarrow \infty$  limit [67]. Thus, the results we have obtained here for such finite- $N$  theories should provide guidance as to how time-dependent mass-generating phase transitions and time-dependent mixings will affect the late-time energy densities for the collections of scalars which emerge in such moose or quiver theories.

It is also worth emphasizing that the results we have derived in this paper reflect the particular KK-derived mixing structure of our model. As a result, we did not observe certain phenomena which may in principle arise for more general systems of scalar fields in the presence of time-dependent mass-generating phase transitions and mixings. For example, it has been shown [18] that in similar scalar systems with more general mixing patterns, parametric resonances can arise which are extremely sensitive to the widths and mixings associated with mass-generating phase transitions and which

“pump” energy density into a particular field or fields during such phase transitions. Such systems may also exhibit so-called “re-overdamping” phenomena [18] in which the total energy density of our system exhibits a time dependence which transcends those normally associated with vacuum-dominated or matter-dominated cosmologies. However, in order for such novel effects to arise, the dynamically generated contribution  $\overline{\mathcal{M}}_{\text{gen}}^2$  to the mass-squared matrix at late times must satisfy the criterion

$$\det \overline{\mathcal{M}}_{\text{gen}}^2 < 0, \quad (8.1)$$

and this criterion is not satisfied within the parameter space of our KK model. However, it is easy to contemplate early-universe scenarios involving multiple scalars in which this condition is satisfied. In such scenarios, parametric resonances and re-overdamping phenomena can then have a significant further impact on both the total abundance of the scalar fields involved and the distribution of that total abundance among these scalars.

There are a number of potentially interesting generalizations and extensions of this work. For example, in this paper we have focused on the case in which the higher-dimensional scalar propagates in a single, flat extra dimension. However, such a flat extra dimension can be viewed as a limit of the more general case of a warped geometry in which the extra dimension represents a slice of anti-de Sitter space [68, 69]. Such warped compactifications have a variety of phenomenological applications, such as providing ways of addressing the hierarchy between the weak and Planck scales [68] as well as the hierarchies amongst the masses of the SM fermions [70, 71]. It would therefore be interesting to examine how our findings generalize to the case of a warped extra dimension. It would also be interesting to consider the further generalization of our results to the case of multiple extra dimensions, both flat and warped. One could also imagine adopting more general initial conditions for our KK modes beyond those in Eq. (2.13), such as might arise if there is an earlier phase of non-trivial dynamics (either in the bulk or on the brane) prior to our mass-generating phase transition.

Another possible avenue for generalization concerns the nature of the cosmological epoch during which we are presuming our dynamics to take place. For example, throughout this paper we have focused primarily on the case in which the universe is effectively matter-dominated (*i.e.*, with  $\kappa = 2$ ) throughout the period of mass generation. Indeed, as discussed in Sect. II, phenomenological constraints on theories with large extra spacetime dimensions are more easily satisfied in LTR scenarios, in which the universe remains matter-dominated until very late times. However, these constraints are considerably weaker in cases in which the compactification scale  $M_c$  is  $\mathcal{O}(\text{TeV})$  or above. Thus, it would also be interesting to consider the case in which the universe is effectively radiation-dominated (*i.e.*, with  $\kappa = 3/2$ ) during



the mass-generation epoch. Cosmologies with other values of  $\kappa$  can be considered as well.

Finally, other interesting extensions of this work involve considering a broader variety of cosmological contexts in which mass generation for our KK modes might take place. Throughout this paper, we have implicitly operated under the assumption that the total energy density  $\rho$  of the KK tower is negligible compared to the critical density  $\rho_{\text{crit}}$  during the mass-generation epoch. Under such an assumption, the back-reaction of the KK tower on the evolution of the spacetime metric is therefore negligible during this epoch. Thus, to a very good approximation, we may view the dynamics of the KK modes studied in this paper as taking place within the context of a particular “background” cosmology which is effectively decoupled from this dynamics and which is therefore specified by a fixed functional form for the Hubble parameter  $H(t)$  as a function of  $t$ . Indeed, such assumptions are valid for a variety of light scalars which receive their abundances from misalignment production — including, by necessity, any such fields which serve as dark-matter candidates. However, one could alternatively consider the opposite regime in which  $\rho \sim \rho_{\text{crit}}$  during the mass-generation epoch. Under such conditions, the back-reaction of the KK tower on  $H(t)$  can be

significant and must be incorporated into the equations of motion for the KK modes. This situation can arise, for example, in scenarios in which these scalar particles play a role in inflationary dynamics or in which they are responsible for additional, later periods of reheating after inflation in cosmologies with non-thermal histories [17]. It would therefore be interesting to study the evolution of the energy densities of the KK modes of our theory in such scenarios.

## ACKNOWLEDGMENTS

We would like to thank S. Watson for useful discussions. The research activities of KRD and JK were supported in part by the Department of Energy under Grant DE-FG02-13ER41976 (DE-SC0009913), while the research activities of KRD were also supported in part by the National Science Foundation through its employee IR/D program. The opinions and conclusions expressed herein are those of the authors, and do not represent any funding agencies.

- 
- [1] R. D. Peccei and H. R. Quinn, *Phys. Rev. Lett.* **38**, 1440 (1977).
  - [2] R. D. Peccei and H. R. Quinn, *Phys. Rev. D* **16**, 1791 (1977).
  - [3] S. Weinberg, *Phys. Rev. Lett.* **40**, 223 (1978).
  - [4] F. Wilczek, *Phys. Rev. Lett.* **40**, 279 (1978).
  - [5] J. Jaeckel and A. Ringwald, *Ann. Rev. Nucl. Part. Sci.* **60**, 405 (2010) [arXiv:1002.0329 [hep-ph]].
  - [6] Y. Chikashige, R. N. Mohapatra and R. D. Peccei, *Phys. Lett.* **98B**, 265 (1981).
  - [7] G. B. Gelmini and M. Roncadelli, *Phys. Lett.* **99B**, 411 (1981).
  - [8] F. Wilczek, *Phys. Rev. Lett.* **49**, 1549 (1982).
  - [9] B. Ratra and P. J. E. Peebles, *Phys. Rev. D* **37**, 3406 (1988).
  - [10] J. Khoury and A. Weltman, *Phys. Rev. Lett.* **93**, 171104 (2004) [astro-ph/0309300].
  - [11] J. Khoury and A. Weltman, *Phys. Rev. D* **69**, 044026 (2004) [astro-ph/0309411].
  - [12] P. Brax, C. van de Bruck, A. C. Davis, J. Khoury and A. Weltman, *Phys. Rev. D* **70**, 123518 (2004) [astro-ph/0408415].
  - [13] A. Dobado and A. L. Maroto, *Nucl. Phys. B* **592**, 203 (2001) [hep-ph/0007100].
  - [14] J. Polchinski, *String Theory, Vols. 1 and 2* (Cambridge University Press, 2001). ISBN 9780521633031 [https://books.google.com/books?id=54DGYyNAjacC].
  - [15] K. Becker, M. Becker, and J. Schwarz, *String Theory and M-Theory: A Modern Introduction* (Cambridge University Press, 2006). ISBN 9781139460484 [https://books.google.com/books?id=WgUkSTJWQacC].
  - [16] M. Green, J. Schwarz, E. Witten, *Superstring Theory, Vols. 1 and 2*, Cambridge Monographs on Mathematical Physics (Cambridge University Press, 1988). ISBN 9780521357524 [https://books.google.com/books?id=ItVsHqjJo4gC].
  - [17] J. Fan, O. Özsoy and S. Watson, *Phys. Rev. D* **90**, no. 4, 043536 (2014) [arXiv:1405.7373 [hep-ph]].
  - [18] K. R. Dienes, J. Kost and B. Thomas, *Phys. Rev. D* **93**, 043540 (2016) [arXiv:1509.00470].
  - [19] E. Witten, *Phys. Lett. B* **149**, 351 (1984).
  - [20] P. Svrcek and E. Witten, *JHEP* **0606**, 051 (2006) [hep-th/0605206].
  - [21] A. Arvanitaki, S. Dimopoulos, S. Dubovsky, N. Kaloper and J. March-Russell, *Phys. Rev. D* **81**, 123530 (2010) [arXiv:0905.4720 [hep-th]].
  - [22] K. R. Dienes, E. Dudas and T. Gherghetta, *Phys. Rev. D* **62**, 105023 (2000) [hep-ph/9912455].
  - [23] K. R. Dienes and B. Thomas, *Phys. Rev. D* **85**, 083523 (2012) [arXiv:1106.4546 [hep-ph]].
  - [24] K. R. Dienes and B. Thomas, *Phys. Rev. D* **85**, 083524 (2012) [arXiv:1107.0721 [hep-ph]].
  - [25] K. R. Dienes and B. Thomas, *Phys. Rev. D* **86**, 055013 (2012) [arXiv:1203.1923 [hep-ph]].
  - [26] O. Wantz and E. P. S. Shellard, *Nucl. Phys. B* **829**, 110 (2010) [arXiv:0908.0324 [hep-ph]].
  - [27] O. Wantz and E. P. S. Shellard, *Phys. Rev. D* **82**, 123508 (2010) [arXiv:0910.1066 [astro-ph.CO]].
  - [28] G. Grilli di Cortona, E. Hardy, J. Pardo Vega and G. Villadoro, *JHEP* **1601**, 034 (2016) [arXiv:1511.02867 [hep-ph]].
  - [29] S. Borsanyi *et al.*, *Nature* **539**, no. 7627, 69 (2016) [arXiv:1606.07494 [hep-lat]].

- [30] N. Arkani-Hamed, S. Dimopoulos and G. R. Dvali, *Phys. Lett. B* **429**, 263 (1998) [[hep-ph/9803315](#)].
- [31] N. Arkani-Hamed, S. Dimopoulos and G. R. Dvali, *Phys. Rev. D* **59**, 086004 (1999) [[arXiv:hep-ph/9807344](#)].
- [32] M. Kawasaki, K. Kohri and N. Sugiyama, *Phys. Rev. D* **62**, 023506 (2000) [[astro-ph/0002127](#)].
- [33] M. S. Turner, *Phys. Rev. D* **33**, 889 (1986).
- [34] K. J. Bae, J. H. Huh and J. E. Kim, *JCAP* **0809**, 005 (2008) [[arXiv:0806.0497](#) [[hep-ph](#)]].
- [35] S. Bauman and K. R. Dienes, *Phys. Rev. D* **77**, 125005 (2008) [[arXiv:0712.3532](#) [[hep-th](#)]].
- [36] S. Bauman and K. R. Dienes, *Phys. Rev. D* **77**, 125006 (2008) [[arXiv:0801.4110](#) [[hep-th](#)]].
- [37] S. Bauman and K. R. Dienes, *Phys. Rev. D* **85**, 125011 (2012) [[arXiv:1112.5631](#) [[hep-ph](#)]].
- [38] D. J. Kapner, T. S. Cook, E. G. Adelberger, J. H. Gundlach, B. R. Heckel, C. D. Hoyle and H. E. Swanson, *Phys. Rev. Lett.* **98**, 021101 (2007) [[hep-ph/0611184](#)].
- [39] R. L. Davis, *Phys. Lett. B* **180**, 225 (1986).
- [40] R. L. Davis and E. P. S. Shellard, *Nucl. Phys. B* **324**, 167 (1989).
- [41] A. Dabholkar and J. M. Quashnock, *Nucl. Phys. B* **333**, 815 (1990).
- [42] T. Hiramatsu, M. Kawasaki, K. Saikawa and T. Sekiguchi, *Phys. Rev. D* **85**, 105020 (2012) Erratum: [*Phys. Rev. D* **86**, 089902 (2012)] [[arXiv:1202.5851](#) [[hep-ph](#)]].
- [43] M. Nagasawa and M. Kawasaki, *Phys. Rev. D* **50**, 4821 (1994) [[astro-ph/9402066](#)].
- [44] S. Chang, C. Hagmann and P. Sikivie, *Phys. Rev. D* **59**, 023505 (1999) [[hep-ph/9807374](#)].
- [45] G. D. Coughlan, W. Fischler, E. W. Kolb, S. Raby and G. G. Ross, *Phys. Lett.* **131B**, 59 (1983).
- [46] T. Banks, D. B. Kaplan and A. E. Nelson, *Phys. Rev. D* **49**, 779 (1994). [[hep-ph/9308292](#)].
- [47] B. de Carlos, J. A. Casas, F. Quevedo and E. Roulet, *Phys. Lett. B* **318**, 447 (1993) [[hep-ph/9308325](#)].
- [48] T. Banks, M. Berkooz and P. J. Steinhardt, *Phys. Rev. D* **52**, 705 (1995) [[hep-th/9501053](#)].
- [49] D. Chialva, P. S. B. Dev and A. Mazumdar, *Phys. Rev. D* **87**, no. 6, 063522 (2013) [[arXiv:1211.0250](#) [[hep-ph](#)]].
- [50] K. R. Dienes, J. Fennick, J. Kumar and B. Thomas, *Phys. Rev. D* **93**, no. 8, 083506 (2016) [[arXiv:1601.05094](#) [[hep-ph](#)]].
- [51] K. R. Dienes, F. Huang, S. Su and B. Thomas, [[arXiv:1610.04112](#) [[hep-ph](#)]].
- [52] K. R. Dienes, J. Fennick, J. Kumar and B. Thomas, to appear.
- [53] K. R. Dienes, S. Su and B. Thomas, *Phys. Rev. D* **86**, 054008 (2012) [[arXiv:1204.4183](#) [[hep-ph](#)]].
- [54] K. R. Dienes, J. Kumar and B. Thomas, *Phys. Rev. D* **86**, 055016 (2012) [[arXiv:1208.0336](#) [[hep-ph](#)]].
- [55] K. R. Dienes, J. Kumar and B. Thomas, *Phys. Rev. D* **88**, no. 10, 103509 (2013) [[arXiv:1306.2959](#) [[hep-ph](#)]].
- [56] K. R. Dienes, J. Kumar, B. Thomas and D. Yaylali, *Phys. Rev. Lett.* **114**, no. 5, 051301 (2015) [[arXiv:1406.4868](#) [[hep-ph](#)]].
- [57] K. R. Dienes, S. Su and B. Thomas, *Phys. Rev. D* **91**, no. 5, 054002 (2015) [[arXiv:1407.2606](#) [[hep-ph](#)]].
- [58] K. K. Boddy, K. R. Dienes, D. Kim, J. Kumar, J. C. Park and B. Thomas, *Phys. Rev. D* **94**, no. 9, 095027 (2016) [[arXiv:1606.07440](#) [[hep-ph](#)]].
- [59] K. K. Boddy, K. R. Dienes, D. Kim, J. Kumar, J. C. Park and B. Thomas, [[arXiv:1609.09104](#) [[hep-ph](#)]].
- [60] L. J. Hall, K. Jedamzik, J. March-Russell and S. M. West, *JHEP* **1003**, 080 (2010) [[arXiv:0911.1120](#) [[hep-ph](#)]].
- [61] M. S. Turner, *Phys. Rev. Lett.* **59**, 2489 (1987) Erratum: [*Phys. Rev. Lett.* **60**, 1101 (1988)].
- [62] E. Masso, F. Rota and G. Zsembinszki, *Phys. Rev. D* **66**, 023004 (2002) [[hep-ph/0203221](#)].
- [63] P. Graf and F. D. Steffen, *Phys. Rev. D* **83**, 075011 (2011) [[arXiv:1008.4528](#) [[hep-ph](#)]].
- [64] A. D. Linde, *Contemp. Concepts Phys.* **5**, 1 (1990) [[hep-th/0503203](#)].
- [65] H. Georgi, *Nucl. Phys. B* **266**, 274 (1986).
- [66] M. R. Douglas and G. W. Moore, [[hep-th/9603167](#)].
- [67] N. Arkani-Hamed, A. G. Cohen and H. Georgi, *Phys. Rev. Lett.* **86**, 4757 (2001) [[hep-th/0104005](#)].
- [68] L. Randall and R. Sundrum, *Phys. Rev. Lett.* **83**, 3370 (1999) [[hep-ph/9905221](#)].
- [69] L. Randall and R. Sundrum, *Phys. Rev. Lett.* **83**, 4690 (1999) [[hep-th/9906064](#)].
- [70] T. Gherghetta and A. Pomarol, *Nucl. Phys. B* **586**, 141 (2000) [[hep-ph/0003129](#)].
- [71] S. J. Huber and Q. Shafi, *Phys. Lett. B* **498**, 256 (2001) [[hep-ph/0010195](#)].